FIBER OPTICS SENSORS

Alfredo Güemes* and Julián Sierra-Pérez†

* Department of Aerospace Materials and Processes, Polytechnic University of Madrid, Madrid, Spain

† Aerospace Engineering Research Group, Pontificia Bolivariana University, Medellín, Colombia

1 Introduction

Fiber optic technology started in 1970's, for long distance telecommunications, and it has experienced an exponential growth during the last four decades. Sensing applications are a small spin-off from this technology, taking profit of developments done for optoelectronic components and concepts.

Optical fibers are cylindrical dielectric waveguides for the propagation of the light, made out from high purity, low loss optical materials, usually silica (Optical fibers made from polymers and other transparent materials are also commercially available). The refractive index of the core (about 1.46 for silica) is slightly higher than surrounding material or cladding, due to the presence of dopants. Light is confined at the core, because optical rays arriving to the interface core/cladding with an angle higher than the total reflectance angle, as defined by the Snell law, will follow total reflections and will remain confined at the core. Only when the fiber is locally bent with a sharp radius, the light may escape. The OF is externally protected from mechanical scratches with a polymeric coating (the 'buffer'), and frequently several optical fibers are bundle together, and assembled with high strength mechanical fibers, such as Kevlar, to make a robust product known as optical cable, that can withstand rough industrial manipulation.

Glass optical fibers have an external diameter of 125 μm (human hair diameter range from 50 to 100 μm), and classify in two main groups: monomode and multimode optical fibers.

Monomode OF, of small core (about 10 μm , depending on the intended optical wavelength). The electromagnetic waves traveling by the core must satisfy the Maxwell equations; the cylindrical contour conditions only allow for a discrete number of solutions, V, dependent on the core diameter, and the wavelength. When V is less than 2.4, only one mode (2 orthogonal

W. Ostachowicz, J. Güemes (Eds.), *New Trends in Structural Health Monitoring*,
CISM International Centre for Mechanical Sciences, DOI 10.1007/978-3-7091-1390-5_5,

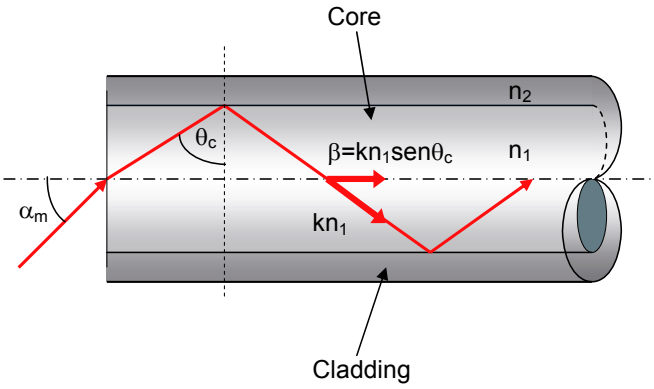

Figure 1. Schematic representation of an optical fiber.

polarizations) propagates through the optical fiber, it is called monomode. Monomode OF offer some advantages for optical communication, such as:

- Optical attenuation is smaller for monomode OF, due to the lower difference of refractive index between core and cladding, requiring a lower concentration of dopants.
- Multimode OF will suffer group dispersion due to different modes traveling at different speed.

The multimode optical fibers have as only advantage a larger core diameter (30 to 100 μm). The larger core makes simpler the alignment with the optical sources and connections. They are preferred when used only as guides for light, as in many medical applications, or in LAN. For sensing purposes they can only be used for intensity based methods.

Optical power loss is extremely small with current OF, in the order of 0.03 dB per kilometer, meaning that 100 km will only divide optical power by two; this is an important requirement for telecommunications. Optical power loss is minimized near the wavelengths of 1300 nm or 1550 nm, where minimum Rayleigh dispersion and minimum infrared absorption is found. From a sensing point of view, optical losses at the fiber are irrelevant, but still 1550 nm is the preferred windows, because optoelectronic components are more easily available.

Our discussion will be mainly restricted to strain and temperature measurements, but fiber optic sensor may be found for many other applications. This would be a first classification for optical sensors, according the physical parameter sensed: chemical, mechanical, electrical, etc. The optical fiber

itself is a pipe for light, transmitting the information, but it may also be sensitive to local changes in the external environment surrounding the fiber, like temperature. With special equipments it is possible to measure the light reflected back along the fiber length and consequently the temperature distribution. The fiber would then act simultaneously as a distributed sensor and as the cable for data transmission, all along its length. This seems to be the ideal approach; it is called 'distributed sensing'; but accuracy and spatial resolution are not good enough for many applications. The approach based on local sensors is more common, either by including into the optical path an external device (extrinsic sensor), or by modifying the fiber during a short length (about 1 cm.), to make it sensitive to the strain or any other parameter. These are the so-called intrinsic sensors, engraved into the fiber, which would go undetectable to the naked eye.

Common advantages of every kind of optical fiber sensors come from its small size and weight; its non-electrical nature, making them immune to EM interference and to electrical noise, also allowing them to work into explosive environments; they usually have a very high sensitivity and a wide operating temperature range. For Smart Structures, local intrinsic sensors are the most appreciated, because of simplicity, minimal perturbation to the host material and accuracy of reading. Multiplexing capability, or the possibility to 'write' several sensors on the same optical fiber, is another highly desired feature. A single optical fiber, 0.25 mm diameter, may afford information of strain readings from 10 to 20 different points at the structure. When compared to the 2 leads required by each electrical strain gauge, a clear advantage is found.

2 Classification of Fiber Optic Sensors

As a wide definition, a sensor is an artifact able to transform a certain physical or chemical magnitude into readable information. Besides the previous topological classification (local/distributed, intrinsic/extrinsic), a more basic classification may be done by the optical parameter. Light is an electromagnetic wave, defined by its frequency, intensity, phase and polarization. The external action to be monitored must change some of the magnitudes that define the optical wave. Based on the kind of these changes, different kind of optical sensors have been developed.

As illustrated at Figure 2, the sketch of a fiber optic sensing system is always very simple: A solid state light source, either monochromatic (laser) or LED (light emitting diode), containing white light as a mixture of frequencies. Light goes though splices and optical connectors, used for assembly/disassembly the optical fibers, and also through couplers and cir-

culators; a 3 dB coupler is a simple artifact where two optical fibers have been fused together, the light arriving by one end is leaving by the other opposite two ends; the couplers work identically in both directions. Light detectors use to be again solid-state, pig tailed optoelectronic components (pig tailed means that an optical fiber is leaving the solid state casing, doing very easy to connect it to the optical circuit).

2.1 Intensity-based sensors

These are the simplest devices among the FOS, and consequently they were among the first attempts, and still are in use as proximity sensors, for damage detection, cure monitoring and hydrogen detection. A stable light source, white or monochromatic, an optical fiber, preferably multimode for higher light power transmission and a sensitive photodetector may compose the whole system.

Commercially available proximity sensors are used for non-contact monitoring of the displacement of rotating shafts with accuracy better than 3 μm. The distance between the cleaved fiber optic end and the moving surface is correlated to the amount of light reflected by this surface, and captured again by the optical fiber (Figure 2).

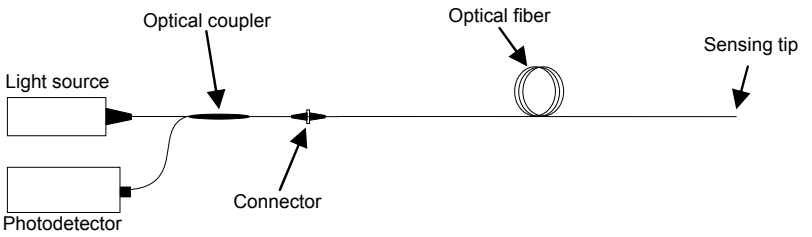

Figure 2. Fiber optic proximity sensors.

Microbending sensors were popular intrinsic sensors for pressure monitoring; they were based on intensity measurements. It is known that light is guided inside the optical fiber because its incidence angle is higher the critical reflection angle at the core-cladding interface, that is always true except for very sharp bends. If the OF is placed between two rough surfaces, a higher pressure promotes higher bending, and consequently higher optical losses. If adequately calibrated, they would afford a measurement of the transversal load on the fiber, by using a local plate, or even the natural roughness of the composite fabrics. Early works were done with this concept, which is currently abandoned; fluctuations of optical power at the

light source, connectors, temperature, etc., make the system rather unreliable. Still the microbending losses must be keep in mind when embedding optical fiber into composite fabrics, because they can fade out the optical signal.

The amount of light reflected at the tip of the optical fiber, according the Fresnel law, is proportional to the refractive index of the external surrounding media (Figure 3); this phenomena has been used for cure monitoring, (the refractive index of the resin is known to change with the cure advancement state), and for hydrogen leakage detection, if the tip was coated with and hydrogen sensitive material, as palladium.

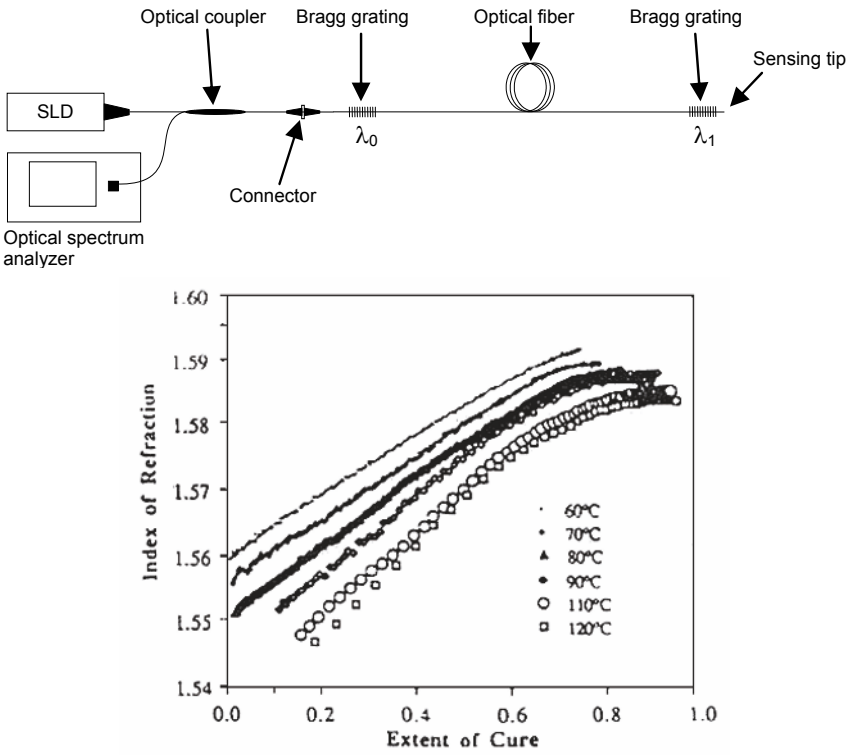

Figure 3. Sketch of cure monitoring systems by intensity based FOS.

2.2 Phase modulated optical fiber sensors, or Interferometers.

Interferometry is the most accurate laboratory technique for precise distance measurements. It has to be bear in mind that direct phase measurements, or the display of the electrical field vs. time cannot be done for the optical wave, as it is done with oscilloscopes for low frequency electrical signals; only light intensity, averaging the power of the electromagnetic field, can be measured. Instead of it, what is done is to split and recombine again the electromagnetic wave. If a continuous monochromatic light wave is divided in two beams (by a partial mirror when dealing with conventional optics, or by a coupler in the case of optical fibers), and these waves travels through different paths before being recombined, any slight difference of path-lengths will cause a delay from one wave to the other, and consequently their electromagnetic fields would not summed up, even they may counteract, and the final result is that output intensity may even cancel.

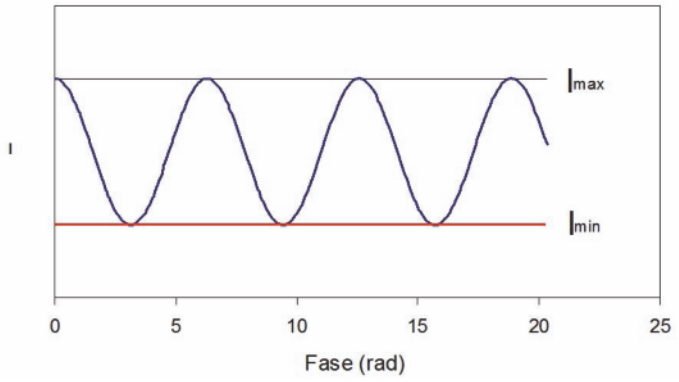

Figure 4. Power output from interferometric measurements.

Interferometers output will move from the power input level to zero level, as sketched in Figure 4, each time the length of any of the two paths increment or decrement in half wavelength (380 nanometers, if the red light of a He-Ne laser was used). This extreme sensitivity to any perturbation in the optical path of any of the two arms makes measurements difficult outside the laboratory environment, because just a local temperature change may cause several maxima and minima drifting. The sensor is the whole length of the optical path of one arm; it is an 'averaging distributed sensor'. Another drawback is that measurements are related to the length when the equipment is put ON, any interruption will lose the reference; also,

there is no direct indication if increment or decrement is happening, and a quadrature technique is needed to identify it.

The Figure 5 sketches the most common optical fiber interferometric architectures, known as Mach-Zender, Michelson, Fabry-Perot, from the names of classical optical interferometry. At the Michelson and Fabry-Perot systems, the light is reflected at the end of the optical fibers, traveling back and recombining again. It has to be emphasized that interferometry requires monochromatic light (laser). It is very simple to arrange these optical sketches with optical fibers, all that is needed are the optoelectronic components, and one or two couplers. In spite of this simplicity, they are very seldom used. A detailed discussion of each of these systems is found at the literature. Fabry-Perot is special in the sense that light travels most of the time by a single fiber, interference is caused among the waves reflected at a partial mirror, and the waves that pass this mirror and are reflected back later. For Smart Structures, a single optical fiber was preferred, because only one ingress point into the structure is required. A lot of work was done for developing a rugged sensor head. Soldering optical fibers after partial coating of the fiber ends did intrinsic sensors. With the development of the Bragg grating sensors, this line of work was abandoned. Extrinsic Fabry-Perot heads, known as 'microcavities' are still commercially available; a precision machined wafer is bonded at the end of the optical fiber, leaving an small air gap, making miniature pressure and temperature sensors.

The Michelson arrangement is employed in the 'white light interferometry', a widely used technique for strain monitoring in civil engineering, which is commercially available by a Swiss company, under the name SOFO. Instead of using a continuous wave monochromatic light, a short pulse is launched through the two arms, the arrival times will be different if their lengths are different, and the photo detector would receive two pulses. If the reference arm can be mechanically stretched to get both pulses coincident, the increase of length in the sensing arm would be known, and from it, its averaging strain is obtained.

2.3 Wavelength based sensors, or Bragg gratings.

These are a kind of local, intrinsic, absolute, multiplexable, interruption immune fiber optic strain sensors, which have concentrate most of the attention since its discovery, at the beginning of the 1990's.

Basic idea is to engrave, at the core of the optical fiber and for a short length (standard FBG length goes from 1 to 10 mm), a periodic modulation of its refractive index. It will behave as a set of weak partial reflecting mirrors, which by an accumulative phenomenon called diffraction, will reflect

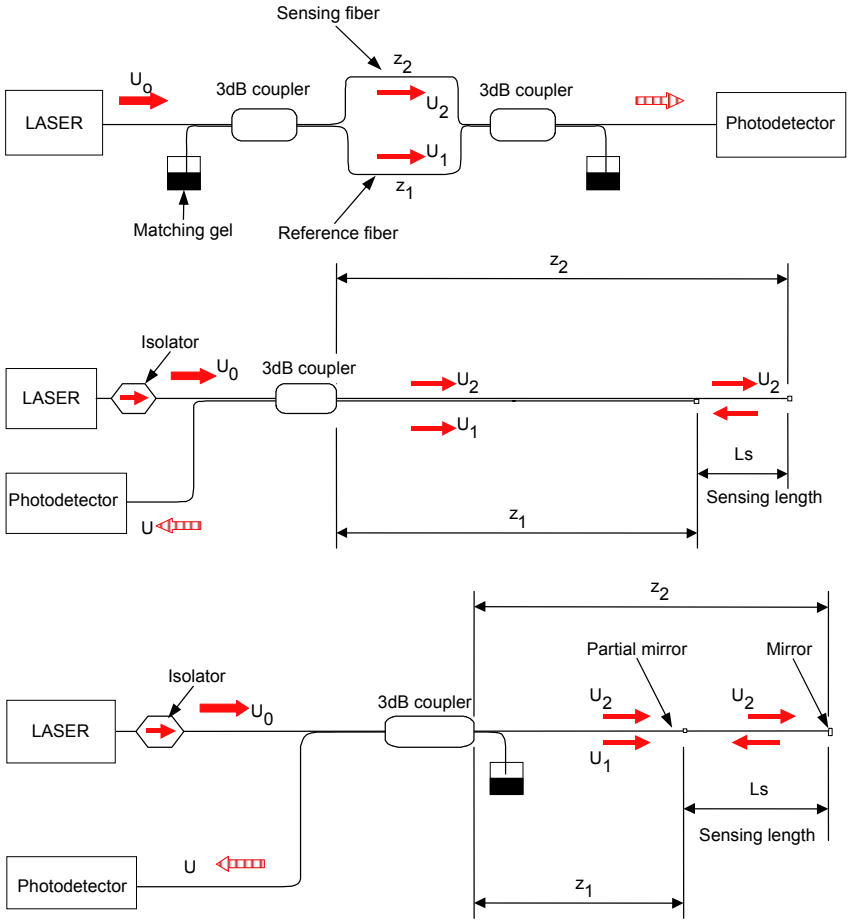

Figure 5. Typical interferometric arrangements (Mach-Zender, Michelson, Fabry-Perot).

back the optical wavelength that is exactly proportional to their spacing. The diffraction law, first established by Bragg and widely used for crystal structure analysis, simplifies under normal incidence to the simple expression:

$$\lambda_b = 2\overline{n_e}\Lambda_0 \tag{1}$$

Where λ_b is the Bragg wavelength, Λ_0 is the pitch or period of the modulation and $\overline{n_e}$ is the average refractive index. The Bragg grating behaves as a very narrow optical filter, as shown at the Figure 6. When a broadband light is traveling through the fiber, the grating promotes that a very narrow wavelength band is reflected back. If the grating is subject to a uniform axial strain, or a uniform thermal increment is applied, the central wavelength of the spectrum reflected by the grating will shift due to changes in the pitch and the refractive index.

Any Optical Spectrum Analyzer (OSA) will be able to detect these changes, and transform it into readable information (Figure 7).

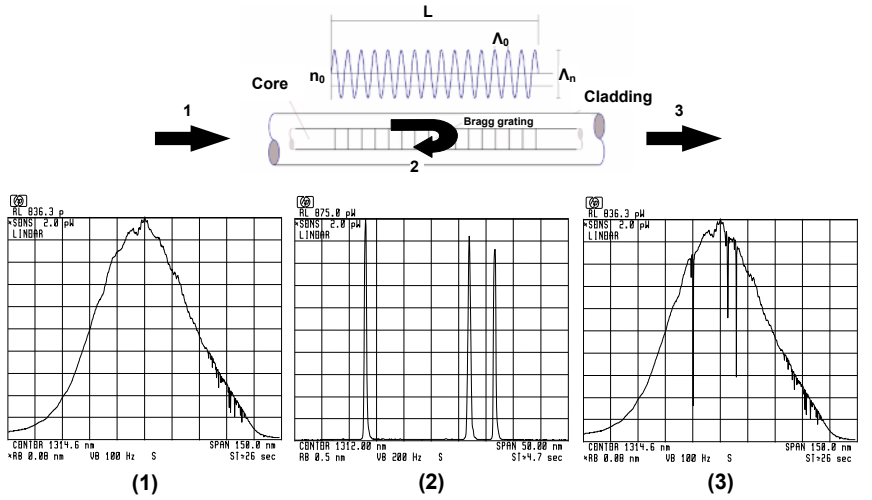

Figure 6. Fiber Bragg grating and operating principle schemes. (1) Intensity spectrum of a broadband source launched into the fiber. (2) Spectra reflected back by three fiber Bragg gratings. (3) Transmissive spectrum after passing the three Bragg gratings.

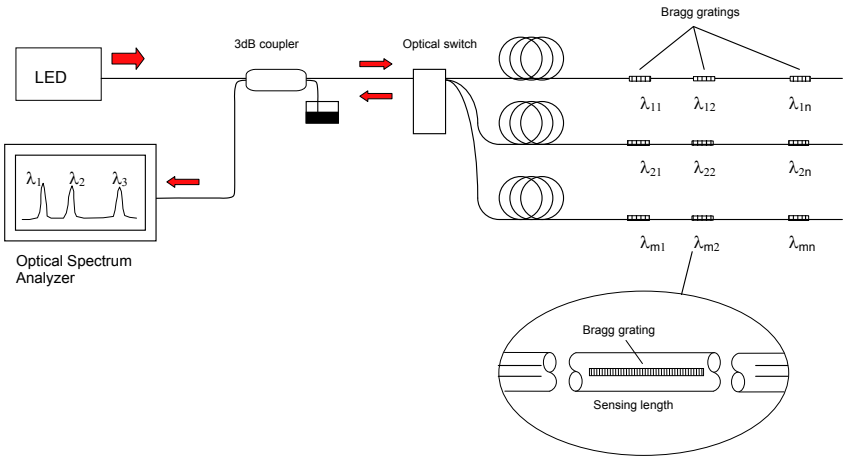

Figure 7. A multiplexed interrogation system for Bragg gratings.

Furthermore, commercially available white light sources have an spectral width around 40 to 60 nm. As the maximum excursion in wavelength is 10 nm for 10.000 $\mu\varepsilon$, several Bragg gratings, centered at different wavelengths, can be written at the same optical fiber, and interrogated at the same time. Multiplexing is easily implemented. The fact that the information is wavelength encoded makes the sensor very stable to aging, allowing absolute measurements of strain after long terms without recalibrating, a common nightmare with standard strain gauges.

3 Fiber Bragg Gratings as Strain and Temperature Sensors

FBG may be bought from several commercial sources, tuned at user defined central wavelength. The only ability required to the user would be to make the optical connections, normally by fusion splices, which require minor investments and training. This is the common approach for mechanical engineers, mainly interested into the usage of this technology for strain measurements. Procedures for manufacturing FBG require high investments and long trained people, and it is useful only for those people interested into the sensor development.

3.1 Response of the FBG to uniaxial uniform strain fields.

When a free FBG is submitted to a uniform uniaxial tension, the photoelastic equations afford a linear relationship among the wavelength drifting and the axial strain, the proportionality coefficient is called sensitivity factor to the axial strain: S_ε

$$S_\varepsilon = \frac{\delta\lambda_b}{\varepsilon_1} = \lambda_b \left[1 - \frac{\overline{n_e}^2}{2}\left[p_{12} - v_f\left(p_{11} + p_{12}\right)\right]\right] \tag{2}$$

Being λ_b the Bragg wavelength, $\overline{n_e}$ its refractive index, v_f the Poisson coefficient and p_{11}, p_{12} its photoelastic coefficients. As an example, for a Bragg grating with the following parameters: Λ_0 of 456.68 nm, $\overline{n_e} = 1.4496$, $v_f = 0.17$, $p_{11} = 0.113$ and $p_{12} = 0.252$ it is found $S_\varepsilon = 1.0598$ x 10^{-3} nm/$\mu\varepsilon$ (943.6 $\mu\varepsilon$/nm) or about 1 pm of wavelength shifting for an strain of 1 $\mu\varepsilon$ (when the central wavelength is about 1300 nm. For 1550 nm, the sensitivity is approximately 1.2 pm)

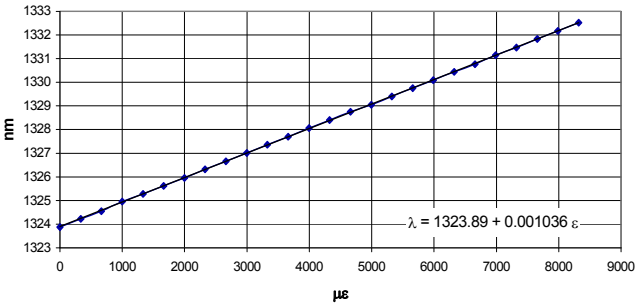

Figure 8. Wavelength shift vs. Axial strain. FBG submitted to uniaxial strain.

Validity of this model is verified with the following experiment, with a FBG bonded on the surface of a unidirectional specimen made from graphite/epoxy AS4/8552. Results are shown at Figure 8, showing an excellent linearity and low dispersion of individual data (standard deviation: 0.01767 nm or about 17.05 $\mu\varepsilon$). Experimentally obtained sensitivity was 1.0363 x 10^{-3} nm/$\mu\varepsilon$, quite close to those previously calculated.

3.2 Sensitivity of the FBG to temperature.

Temperature influences the behavior of the FBG by a linear thermal expansion of the grating, and also by changes in its refractive index. Both

effects may be summarized in the following expression:

$$\frac{\delta\lambda_b}{\lambda_{b,0}} = (\alpha + \xi)\,\delta T \tag{3}$$

Typical values for these coefficients are 5 to 5.5 x 10^{-7} for the thermal expansion of the silica, and one order of magnitude higher (8 to 10 x 10^{-6}) for the thermo-optic coefficient. Changes in the refractive index are the main factor, and both coefficients are rather constants for a wide temperature range (-50 °C to 500 °C). These values mean a drifting of about 1 nm per 100 °C, for a grating with an unperturbed wavelength of 1300 nm. For accurate strain measurements, temperature effects need to be corrected, similarly to common strain gauges.

First exposure of the grating to high temperatures (over 100 °C) causes a partial loss of reflectivity of the grating, and also a permanent drifting in central wavelength. To get a repetitive response at high temperatures, gratings need to be annealed. Once this is done, FBG work reliably at high temperatures, up to 800 °C.

At cryogenic conditions, for temperatures down -223 °C, the coefficients are no longer constants, and the linearity is lost. At liquid helium (-268.95 °C) both coefficients are almost zero and the wavelength variation with temperature is negligible under these conditions.

3.3 Response of the FBG to non-uniform uniaxial strain field.

The reflected spectra by an unloaded standard Bragg grating is a very narrow (0.1 nm) symmetric Gaussian peak. This spectra may be acquired by an OSA (Optical Spectrum Analyzer), representing the collected power vs. wavelength. This peak would simply moves back or forwards when the FBG is uniformly loaded, and its pitch, or internal periodic modulation, is changing accordingly. If the FBG would be submitted to two different strain levels along its length, two different peaks of lower height must be expected. In general terms, an strain gradient along its length will distort the reflected peak. The direct problem, or how to calculate the shape of the reflected peak corresponding to a given strain field can be easily done by the Transfer Matrix Formalism (TMF). The TMF is a numerical method to solve the coupled mode equations for aperiodic grating structures. Figure 9 shows the calculated spectra for a linear gradient, and the experimentally obtained values with a simply supported beam reproducing this strain gradient are shown in the Figure 10. The agreement is very acceptable.

The inverse problem, or to obtain the strain profile from the acquired spectrum, is not as straightforward, information of the intensity and phase

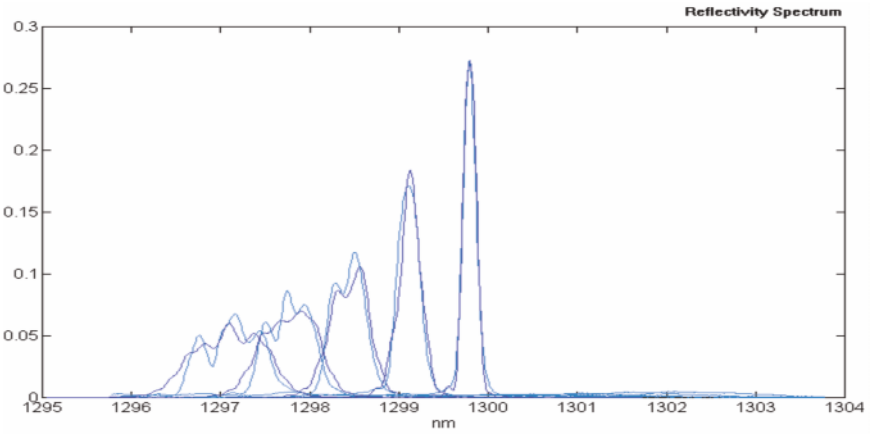

Figure 9. Real and simulated spectra of the grating attached to the beam in several load conditions.

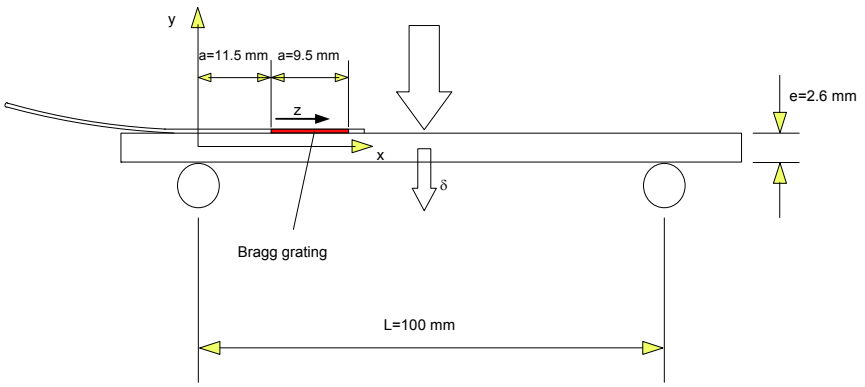

Figure 10. Experimental arrangement for the calibration of the sensor.

would be required. Even some algorithms have been proposed, a simpler approach to obtain the strain gradient is to engrave several short length FBG (1 mm each) as closely located as requested by the experiment.

3.4 Response of the FBG to transverse stresses.

The situation that complicates the suitability of fiber Bragg gratings is their response to non-unidirectional stress. The first sign of this effect appears in fiber Bragg gratings embedded in a thick graphite/epoxy laminate cured at high temperature. Several gratings used to monitor strain and temperature during the cure process split in twin spectra during the cooling of the laminate. Bending of the fiber shows an exchange of optical power between the two sides of the twin spectra, pointing out a birefringence of the fiber promoted by the presence of strong residual stresses inside the laminate.

A transverse stress field applied to the grating promotes a birefringence that modifies the isotropic optical structure of the fiber, generating two principal directions of polarization, with two different refractive indexes. The fiber Bragg grating verifies two different Bragg conditions, and the optical spectrum of the grating splits in two. By using a fiber Bragg grating written in the core of a standard low-birefringence optical fiber, immersed in a general stress field, it would not be possible to separate the components of the stress field using the spectral information of the grating. These phenomena have been experienced by many authors and several methods have been proposed to avoid, or minimize them: use of special fiber, encapsulate the gratings, etc.

Assuming an FBG submitted only to transversal stresses, a FEM analysis can be done to obtain the strains at the core in radial directions, the two refractive indexes and the corresponding wavelength drifting. The most immediate result that can be induced is that distance between the two peaks of the splitted peak is only affected by the transverse stress applied to the fiber, and is proportional to it (Figure 15), where $k \cong 70$ x 5.8514 GPa is the coefficient of proportionality, λ_0 is the Bragg wavelength of the non-perturbed grating, $\delta\lambda_2$ and $\delta\lambda_3$ are the wavelength shifts of the splitted peaks.

It is also possible to obtain an expression for the longitudinal strain of the grating as a function of the displacement of the wavelength of one of the peaks and the distance between the two peaks, $\delta\lambda = \delta\lambda_2 - \delta\lambda_3$, that is:

$$\varepsilon_1 = 1.25\frac{\delta\lambda_2}{\lambda_0} + 0.46\frac{\delta\lambda}{\lambda_0} \tag{4}$$

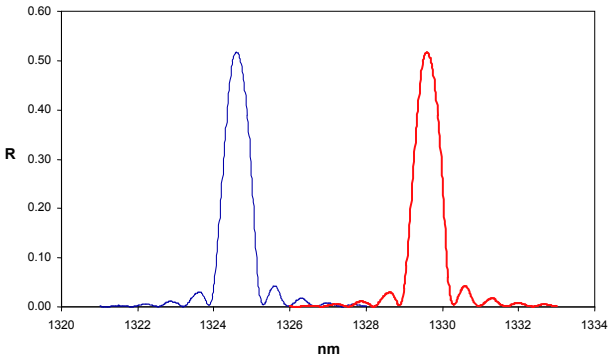

Figure 11. Spectra of a fiber Bragg grating bonded in an aluminum beam: unloaded (narrow line) and submitted to a uniform longitudinal strain of 5000 mε (thick line). The 'ideal' behavior of a grating.

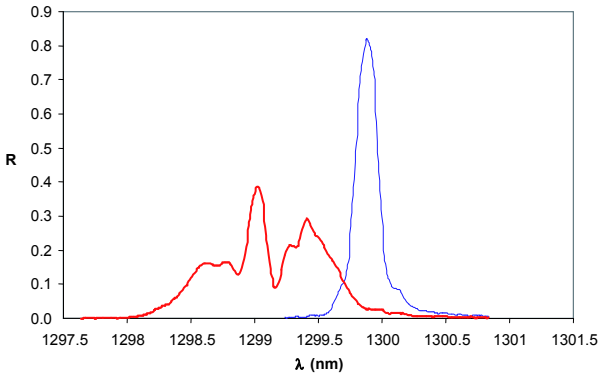

Figure 12. Spectra of a fiber Bragg grating embedded in a unidirectional composite laminate near a bonded joint: unloaded (narrow) and submitted to longitudinal load (thick). The distortion is due to strain gradients.

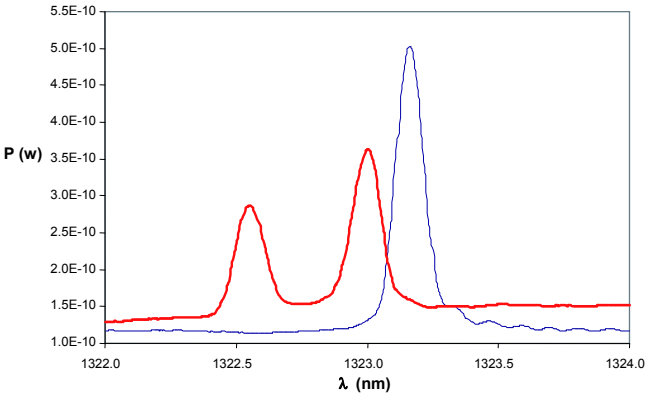

Figure 13. Spectra of a fiber Bragg grating before (narrow) and after being embedded in a thick quasi-isotropic laminate cured in autoclave (thick); the splitted red spectrum shows the effect of strong transverse stresses over the grating.

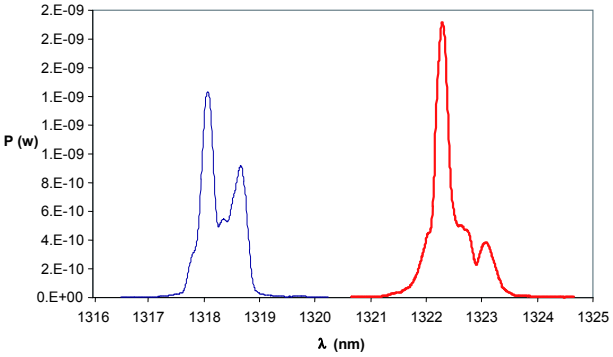

Figure 14. Spectra of a FBG embedded in a composite beam made with fabric and cured in autoclave: unloaded (narrow), shows the typical splitting of a biaxial stress state; loaded (thick), shows the effect of a complex non-uniform biaxial stress field.

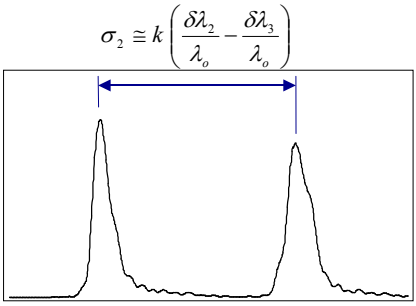

Figure 15. The distance between the two peaks of the splitted peak is only affected by the transverse stress applied to the fibre, and is proportional to it.

In order to prove the validity of these results, two different experimental tests have been implemented. The first one, very simple, uses the well-known thermal expansion of the aluminum to prove the importance of the effect of transverse stresses over fiber Bragg gratings in apparently very simple applications. The second test, with four gratings embedded in different positions in a graphite/epoxy laminate, will allow evaluating the effect of the residual stresses generated in a laminate during the cure processing.

The use of fiber Bragg gratings to monitor strain distributions in bonded joints in aluminum elements using high temperature adhesive film was one of the first applications in which the importance of transverse stress in their spectral response appears clearly. The following test has been configured as an illustrative example of this behavior, and shows the necessary precautions that have to be taken when using this technology in applications in which temperature or external loads can promote transverse strain fields over the gratings.

Figure 16 shows a bare fiber Bragg grating 10 mm long written in photosensitive fiber and submitted to thermal stabilization at 300 °C during 2 hours has been bonded in a beam of AA5083 aluminum using an epoxy adhesive film. The adhesive has been cured using a standard cycle shown in the Figure 17(1).

Figure 17(2) shows the evolution of the Bragg wavelength of the grating with the temperature during the curing cycle. The wavelength of the grating increases during the first part of the heating stage, according the curve wavelength/temperature of a free grating, as a single peak.

At 170 °C, there is a discontinuity in the slope promoted by the fast

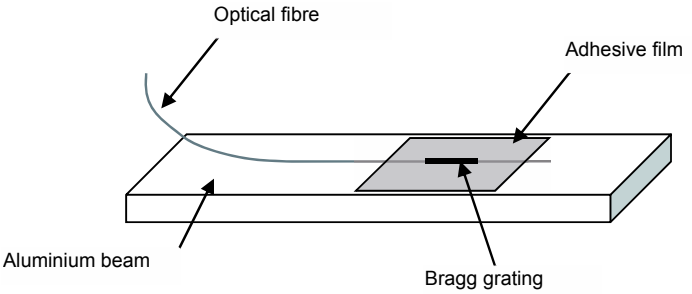

Figure 16. Schematic of aluminum beam with a fiber Bragg grating bonded using adhesive film.

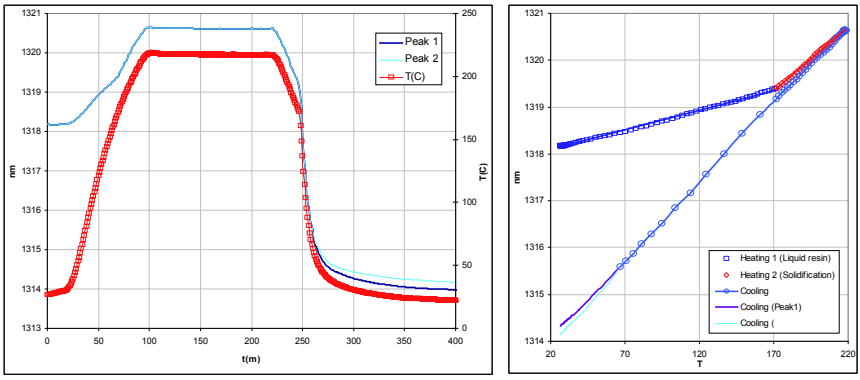

Figure 17. (1) Evolution of temperature and the wavelength of the Bragg wavelength of the grating during the curing cycle. The spectrum of the grating split in two during the cooling of the specimen; (2) Evolution of the Bragg wavelength with temperature during the curing cycle.

gelification of the resin, which forces the grating to follow the thermal expansion of the specimen. During the cooling, the wavelength decreases with this last slope, but the grating split in two at 70 °C (the discrimination of two different peaks depends on the resolution of the spectral analyzer used) due to the thermal transverse strain of the beam.

The wavelength shift of a grating bonded to an aluminum specimen with a linear expansion coefficient α_{AL} is given by:

$$\delta\lambda_b = \delta\lambda_{bT} + \lambda_{b0}\,(\alpha_{AL} - \alpha_f)\,\delta T \tag{5}$$

Where $\delta\lambda_{bT}$ is the wavelength shift of the free Bragg grating with the temperature and α_f is the linear expansion coefficient of the optical fiber. The values of linear expansion coefficient for the AA5083 aluminum and the optical fiber are known (α_{AL} = 23.5 x 10^{-6} K^{-1} and α_f =5.5 x 10^{-7} K^{-1}), then the value calculated for the final Bragg wavelength of the grating after the cooling is 1314.20 nm, whereas the empirical result obtained was 1314.19 nm for a cooling from 180 °C to 20 °C, demonstrating the accuracy of the model.

In this case, it is difficult to find an immediate quantitative relationship between the transverse shrinkage of the aluminum specimen and the shift of the spectrum of the grating due to the complex host/adhesive/sensor interaction.

A graphite/epoxy laminate specimen made of 24 plies of unidirectional T300/F155 prepreg tape with the following configuration: [[90]8[0]4]s, 150 x 125 x 8 mm, cured in a hot plates press at 180 °C in an quasi-isothermal cycle (the specimen was introduced in the press with the plates at the curing temperature. Four bare fiber Bragg gratings were embedded in the laminate parallel to the reinforcing fibers, two in the middle plane (gratings 1 and 2) and two in the outer laminae (gratings 3 and 4). Spectra of the four gratings at different stages of the process are shown in Figure 18.

With these data, and using the expressions obtained from the photoelastic model, the values reported in Table 1 of strains and stresses are calculated:

In the Table 1 a 'f' has been added as a subscript to remark than these results are the strains and stresses at the core of the grating. Strains in the laminate and the optical fiber should be roughly the same, but the agreement in this case is only qualitative for the transverse direction, and how to use FBG to obtain internal residual stresses in composite laminates is still an interesting research topic. The most common approach, to avoid these complexities, is to cover the FBG with some coating that dampen the transverse stresses, reducing or eliminating the peak splitting.

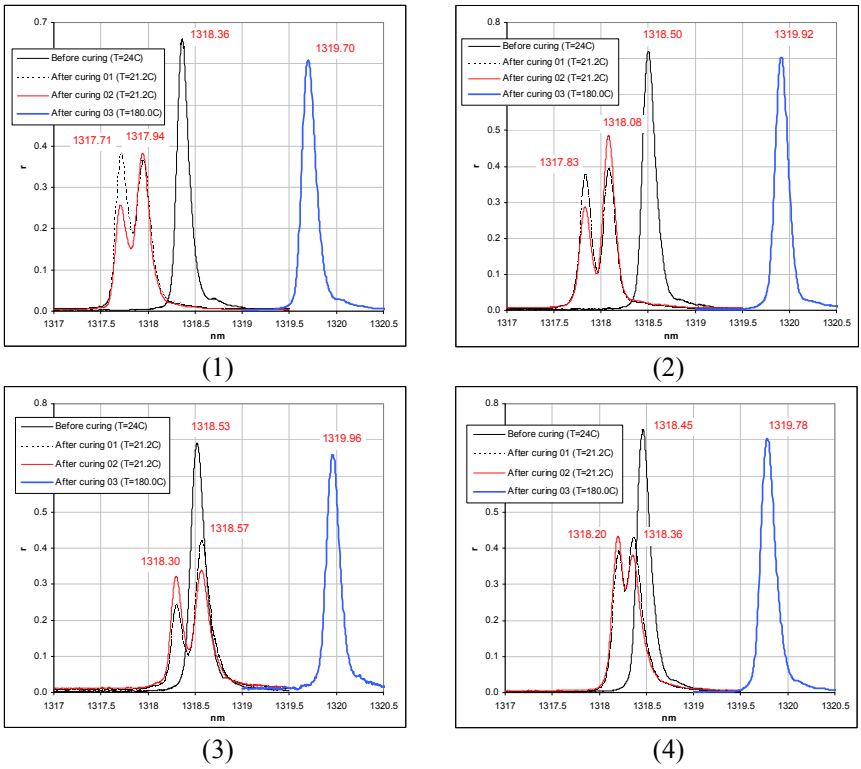

Figure 18. Spectra of the four gratings in different moments of the process: grating at 24 °C before curing, grating at 180 °C after curing (still single peak), and grating at 21.2 °C after curing (two peaks).

Table 1. Residual strains and stresses calculated using the photo elastic model.

Grating N$^{\underline{o}}$	σ_{1f} (MPa)	σ_{2f} (MPa)	ε_{1f} ($\mu\varepsilon$)	ε_{2f} ($\mu\varepsilon$)
1	-15	71	-385	1057
2	-19	78	-453	1155
3	13	84	-20	1167
4	24	50	-87	705

3.5 Commercial FBG interrogation systems.

The interrogation scheme given at Figure 7, using an OSA (Optical Spectrum Analyzer), is too slow and bulky for practical applications; besides it, getting the detailed spectrum is not usually required, information of the peaks wavelength is enough for most of the practical cases.

FBG interrogation methods can be classified by the measurement frequency. Conventional systems use wavelength sweeping by mechanical moving parts by piezoelectric actuators, such as a tunable laser source or a tunable Fabry-Perot filter; they are used for the wavelength interrogation with the measurement frequency under 1 kHz, which is enough for most of the common mechanical applications.

For the measurement frequency over 1 kHz, which is required for strain measurements under impact conditions, or for the analysis of elastic waves generated into the structure, Bragg wavelength shifts should be converted into optical power through a certain type of optical filter without introducing any mechanical moving parts. A very simple and economic solution is obtained by a diffractive grating associated to a CCD array, even the resolution is not as good as with the former techniques.

The higher speed is obtained by using wavelength dependent filters, as a LPG or a AWG, being able to reach 1 MHz, as the only limit is the speed of the photo detector. In these cases, the sensing FBG must have a wavelength centered at the window of the filter, and the span is limited to the window width; these conditions limits severely the multiplexing capability, usually based on different central wavelengths.

4 Structures With Embedded Fiber Bragg Gratings

The possibilities of structural integration do not only depend on the sensor characteristics. The structural material, from now onwards denominate 'host', also have to fulfill a set of requirements to allow the integration of fiber Bragg gratings, without disturbing the manufacturing process. Host has to be immune to the presence of the optical fiber, so that its mechanical properties or its structural integrity is not modified.

Although the fiber optic, and therefore the sensors, can be bonded externally to any material on any structure, the concept of Smart Structure carries inherently the concept of integration. Some of the advantages associated to embedding fiber optic sensors are:

- Increased survival possibilities of the optical fiber and integrated sensors, intrinsically brittle, that would be protected by the external structure.

- The existence of an intimate sensor/host union.
- The absence of external wiring, important not only from the aesthetic point of view, but also allowing its use for applications that require clean surfaces, as it is the case of aeronautical structures.
- The possibility for internal monitoring of the structure, in places which cannot be reached by conventional sensors, or would be too intrusive by their size and by the high number of wires that usually are necessary to route until them.

A full integration of sensors into the host material is limited by the material nature and by the manufacturing processes. For example, the maximum temperature for silica fiber (without external shell) is about 900°C, limiting its possibility for embedding in metals and metal matrix composites. Concrete structures, and advanced composite materials with polymeric matrix are more adequate for integration purposes.

Manufacturing process of structural elements also limits the use of embedded fiber optics, because it is necessary to avoid potentially aggressive operations, such as high pressures application, shear stresses and very small chamfers. Another critical factor is the survival of fiber terminals to connect structural elements each other, for the output monitoring systems.

For using fiber Bragg grating as strain sensors it is necessary to have the maximum information possible about its surroundings in order to establish basic criteria to guarantee the accuracy, repeatability and stability of the measurements.

The main mission of the coating is the mechanical and environmental protection. Commonly used materials for coating optical fiber are polymers, acrylate or polyimide The coating characteristics are also very important because the stress and strain transmission from the structural element to the fiber is made through it, and its characteristics will impose the response of the sensor/structural element. Standard optical fiber has an acrylate coating, with low elastic moduli, low bare strength, oxidizing at temperatures used for curing composite materials (around 180°C). Polyimides have greater rigidity and bare strength, and do not degrade to these temperatures, reason why it is preferred for embedding in composite materials.

Some factors influencing the response are:

- The coating thickness: it has to be sufficient to isolate from cross-sectional stresses, but not excessive, since it could be intrusive and could delay the transmission of longitudinal deformations.
- Its tolerance to the adhesive cure process or the matrix in which the fiber is embedded, decreasing its degradation to high pressures and temperatures.

– Its chemical compatibility with host material, and degradation resistance in humidity conditions.
– Its rigidity, as nearest as possible to the resin matrix.

4.1 Orientation of the optical fiber optic respective to the reinforcement fibers.

The main factor in the behavior of fiber/host is, for the case of composite materials with long fiber reinforcement, the orientation of the optical fiber respective to the reinforcement. The monomode fiber used in Bragg grating sensors is 125 μm diameter, approximately the same thickness as a composite material lamina. In the surroundings of the optical fiber, a resin-rich zone appears, named resin pocket (Figure 19). In weave laminates the determination of resin pocket geometry is very difficult, by the complexity of the phenomena implied in its formation. In the case of tape laminates, resin pocket size is reduced when the optical fiber/reinforcement fiber angle is reduced, and disappears when it is embedded longitudinally to them.

The resin pocket geometry and size depends on the reinforcement fibers orientation of adjacent sheets to optical fiber. The best configuration is optical fiber embedded parallel to the reinforcing fibers. In this way the resin pocket size is null, and the optical fiber interference with the laminate is practically null. It will be necessary to set reduced points in which the angle optical fiber/reinforcement is not null and identify them as possible sensitive zones.

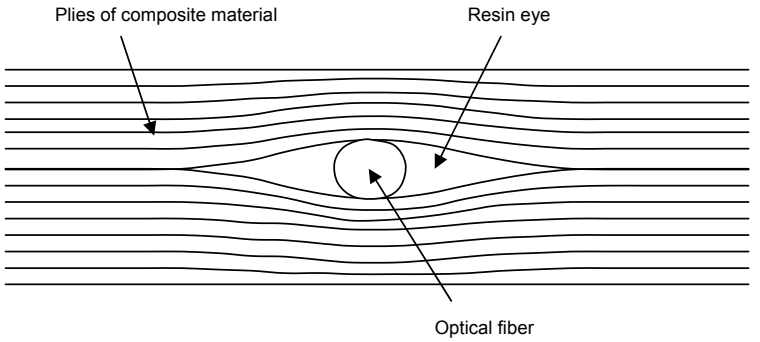

Figure 19. Sketch of the laminate cross section, showing the 'resin eye'.

It is evident that the resin pocket, besides to create a laminate zone without reinforcement material, causes a distortion of the stresses field which

may initiate a delamination process.

In laminates made with fabrics, the fiber weft, added to the applied pressure during the curing process and the differential contraction that appears during cooling may cause a fiber breakage or, if the fiber has survived the application of pressure, the build-up of a complex stresses fields and residual strain around the Bragg grating, making very difficult to analyze its response. After a lot of tests on integration of Bragg gratings in materials we concluded that best way to use Bragg gratings in this type of laminates is surface bonding or embedded between unidirectional tapes that protect the optical fiber.

4.2 Ingress/egress from the laminate.

The input/output ends of the fiber are considered critical points for mechanical interference of the optical fiber with the structural host element. Standard procedures for input/output of the optical fiber from the composite materials still do not exist. It is due to the difficulty to edge machining the composite materials parts with optical fiber terminals or connectors leaving the laminates edges. The developments carried out during the last decade aim at two possibilities:

Use of composite materials manufacturing techniques that avoid the need of later edge trimming (RTM, SMC, RIM, etc.) and would allow semi-embedded connectors on any surface of a laminate. Their effect on the mechanical behavior of the part, and therefore the precautions to take from a point of view of the fiber survival, will be similar to conventional rigid inserts.

Output by means of pig-tails through the laminate flat surfaces, which obviously do not require any later manipulation. The effect on the laminate characteristics will depend on several factors: laminate configuration in the surroundings of the output, size and rigidity of the cable, etc.. The existence of a low module inclusion in a contour piece zone is not an optimal solution for high structural requirements applications, mainly in aeronautical applications, reason why it would have to be restricted to light loaded elements or laboratory applications. In the case of outputs by rigid inserts, the precautions to be taken will be the adapted to these kinds of elements.

5 Examples of Applications in Aeronautics and Civil Structures

Although not still incorporated to series production, neither accepted for Certification procedures, a large number of demonstrations can be found

in the open literature. The practical details for the implementation of two structural elements instrumented with fiber Bragg gratings are detailed next, illustrating the special precautions to be taken, and the results obtained.

5.1 Stiffened panels with embedded fiber Bragg gratings.

Three stiffened panels with co-cured stiffener webs were manufactured by means of manual lay-up and autoclave curing. This structure could simulate a portion of the skin panel of a tail plane or a wing of a small aircraft. Two of the panels (panels number 1 and 2) were instrumented with optical fiber Bragg grating sensors bonded on the stiffeners and back-to-back on the skin surface. The other panel (panel number 3) was provided with two embedded optical fiber sensors in each stiffener. Additionally FBGs and strain gauges were bonded on the stiffener webs and on the skin back to back.

The panels have a dimension of 560 mm x 280 mm with 3 blade stiffeners of 20 x 20 mm cross-section situated in the middle line and at 105 mm on the left and on the right from the middle line. Skin thickness is 1 mm and stiffener thickness 1.6 mm. Fiber lay-up of the panels has been optimized, being in panel 3 skin: $(\pm 45^{\circ}_{(f)}, \pm 45^{\circ}_{(f)}, 0^{\circ}, \pm 45^{\circ}_{(f)}, \pm 45^{\circ}_{(f)})$ and in the stiffener: $(\pm 45^{\circ}_{(f)}, 0^{\circ}, 0/90^{\circ}_{(f)}, 0^{\circ})_S$ using a combination of unidirectional and fabric (f) carbon fibers.

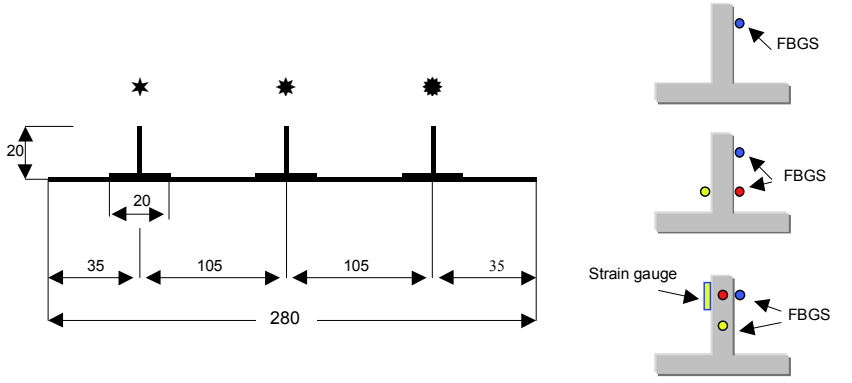

Figure 20. Dimensions of the panels with details of the sensors position in panel 1, 2 and 3.

For manufacturing the stiffened panels a toughened epoxy prepreg mate-

rial Hexcel A-193-P/8552S carbon fabric and AS4/8552 unidirectional tape with AS4 high-strength carbon fiber were employed.

The panels were manually laid-up over a reinforced elastomeric mold made of Airpad polyacrylic rubber (Airtech). The elastomeric mold turned out to be very suitable for embedding the optical fibers in the laminate. The elastic rubber surface of the mold enables the optical fibers covered by their protection tubes to be guided between the laminate and the mold and protects them from high-pressure concentrations. The applied curing cycle was the standard one recommended by the prepreg manufacturer (180 °C/ 6 bar, 2h). For panel 3 a lower pressure of 4 bars was applied. Panel edges were machined with a diamond disc saw. After edge machining, panel edges were potted into an epoxy/gypsum mixture inside a normalized U-transverse section steel profile (80 mm width, 45 mm high) to ensure uniform loading (Figure 21).

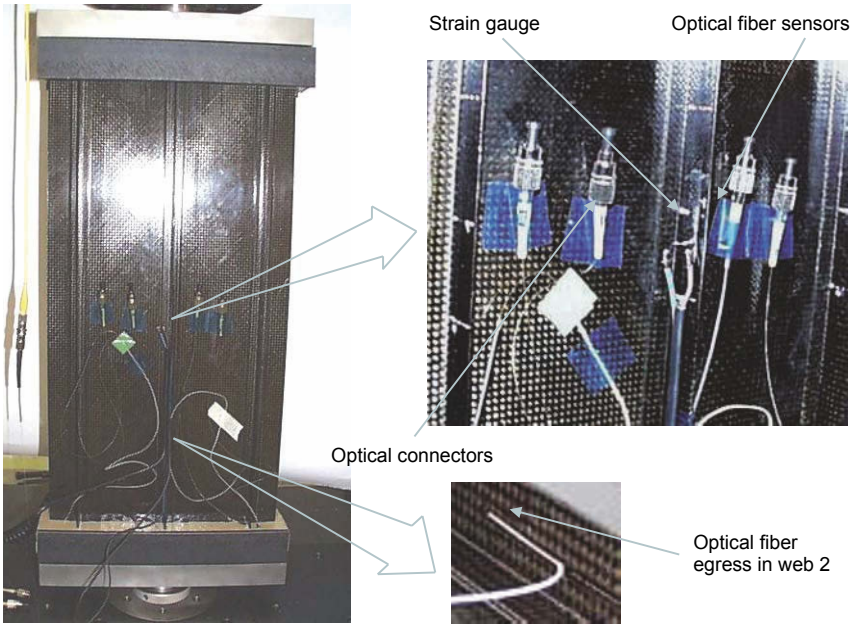

Figure 21. Integration of optical fibers in the stiffener webs

The optical fiber sensor used is a 230 mm long portion of photosensitive optical fiber with a 10 mm long Bragg grating sensor zone located at 65 mm from the end of the photosensitive fiber. For panels 1 and 2 sensors

were bonded by means of a cyanate adhesive to the slightly grounded and degreased surface of the panel. The photosensitive fiber was spliced with a conventional single-mode fiber provided with an optical connector.

In panel 3 a 165 mm long photosensitive fiber was spliced with an 800 mm long single-mode conventional optical fiber. Two FBGs were embedded in the web of each one of the three stiffeners of the panel. The optical fibers were placed between the two central 0° layers and parallel to the reinforcement fibers. Their sensing zone was located at mid-span of the stiffener. Embedding the optical fibers between 0° prepreg layers ensures that they will not be destroyed during the consolidation process and that they will provide a reliable sensor signal that will not be spoiled by the lobed curve surface of the fabric layers. A tiny hole was made passing through the laminate to enable the optical fiber to get out of it. A 0.8 mm diameter PTFE tube was used to protect and guide the two optical fibers in each web out of the laminate. This tube was sealed with silicone to prevent resin contamination. A lead of about 25 mm of this PTFE tube was left inside the laminate to guaranty a good protection of the fiber at the point where it comes out from the laminate. The rest of this PTFE tube was guided between the laminate and the mold coming out of the mold at its front side. A long portion of the protected optical fiber was left outside the laminate and a connector was fixed to it after curing.

Additional FBGs and conventional strain gauges were surface bonded on panel 3 to verify the strain measurements of the embedded FBGs. Conventional strain gauges were also bonded on the skin to determine the skin buckling. The strain gauges were bonded in all the webs on the left web site at the same location than the upper embedded FBGs; FBGs were bonded on the right web side. In the middle web also additional gauges were bonded in front of the lower FBGs on both sides of the web. All the sensors survived the manufacturing of the part, showing clearly defined spectral peaks with no significant distortion due to complex local strain fields caused by residual stresses.

To verify the exact geometrical position of the embedded optical fibers inside the stiffener webs several X-ray images have been taken from panel 3. The images showing 300 mm of the stiffener length including the fiber egress. A micro focus X-ray system has been used operating at a low voltage level to obtain sufficient high resolution that enables the detection of the small optical fiber inside the composite. Figure 22 shows the X-ray image of stiffener web 3. The two optical fibers can be clearly identified within the composite. On the left side the fiber egress with the protective Teflon tube can be seen. The resolution is high enough to detect not only the fiber path but also possible optical fiber cracking within the composite.

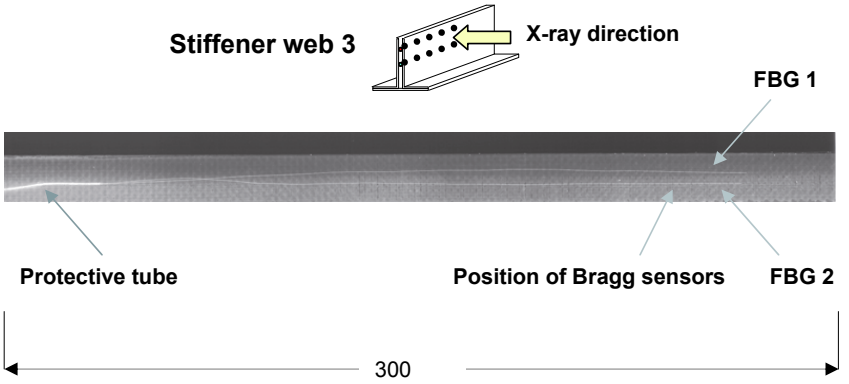

Figure 22. X-ray image of stiffener web 3 in panel 3 indicating the position of the optical fibers and the protective tube at fiber ingress.

Compression tests at room temperature were conducted for the three panels For panels 1 and 2 the sensors worked correctly up to the panel failure. In the explosive rupture the splice of the photosensitive and the conventional single-mode fiber broke at almost every sensor. Fixing an optical connector directly to the photosensitive fiber would leave the sensors operative even after rupture of the panel.

In the case of panel 3 the six FBGs were embedded in the centerline of the stiffener web so that they were able to measure tensile/compression strains but not transversal bending or twisting of the web. At the beginning of the compression test all the sensors detect the same compressive strain up to the moment when buckling occurs at a strain level of 800 $\mu\varepsilon$. A large bending strain in the skin can be noticed by the bifurcation of the sensor signals of the bonded strain gauges. Skin buckling increases the load that has to be carried by the stiffeners and induces also a twisting and transverse bending of the stiffeners. With increasing load, longitudinal bending of the web occurs. Figure 23 shows the strain measured with the upper embedded FBGs, the bonded FBGs and the bonded strain gauge of the stiffener web 1, 2 and 3. The measurement of the skin bonded strain gauges is also included in the graph to indicate the skin buckling.

5.2 Concrete beam repair

Advanced composites offer some advantages over traditional procedures for repairing concrete structures, due to their optimal corrosion properties,

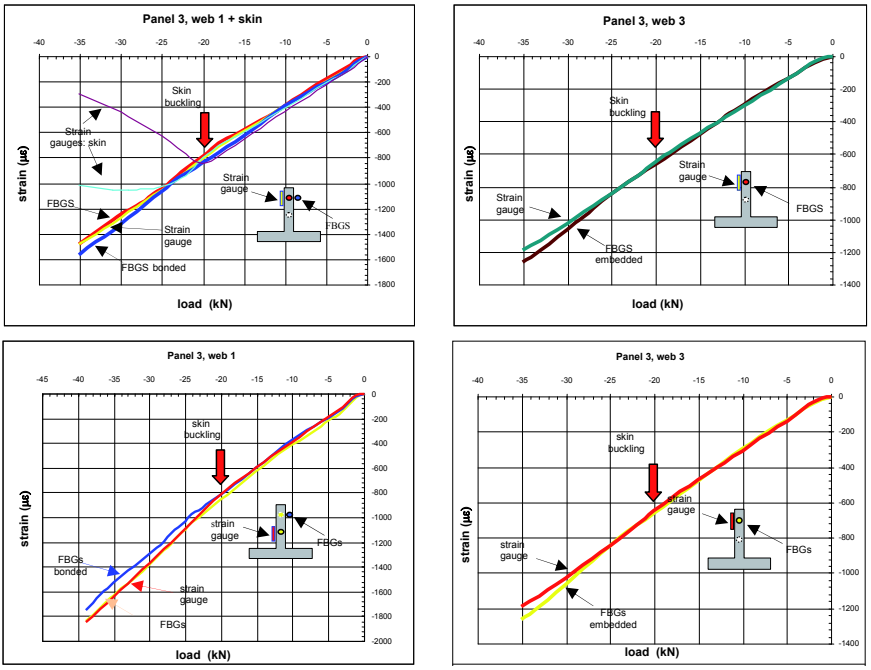

Figure 23. Strain vs. load values from the FBGs and strain gauges of stiffener web 1 and 3.

low weight and decreasing costs. Thin cured laminates may be externally bonded or dry fabrics can be applied in situ.

On the other hand, Bragg gratings show the aforementioned advantages when compared to conventional strain gauges: absolute measurements, spectrally encoded output, no EMI, no drift (long-term stability), low size, multiplexing capability and their ability to be embedded into laminates without degradation or detriment effects.

The combination of both techniques is easy and offers important advantages. The long- term mechanical behaviour of the repair may be checked and information on environmental degradation could be obtained. On the short term, information on the stress transfer from the concrete to the laminate is obtained, and the validity of models is verified.

Tests description. A reinforced concrete continuous beam with two spans (7.2 m + 7.2 m), representative of current in-service civil engineering struc-

tures, was loaded up to failure and repaired. After removing loose concrete near the cracks, new concrete was poured. Composite patches, made of two layers of carbon fabric, in-situ impregnated with room temperature epoxy resin, were extended over the crack locations, to transmit the load from the discontinued steel bars. Bragg gratings were placed with the fabrics, both in the internal and external surfaces. External pre-stressing was added to increase the failure load. Arrangement is shown in Figure 24

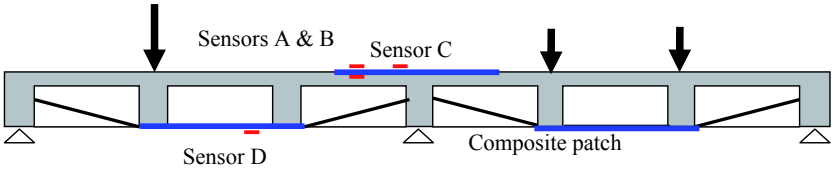

Figure 24. Test arrangement and Bragg grating locations.

Results. Strain vs. Load is plotted in Figure 25, obtained with strain gauges and FOS. Coincidence is very satisfactory, even at the non-linear region of the concrete beam. Damage starts near 80 kN, still with considerable residual strength. Worth to mention that ultimate load of the repaired beam (156.6 kN) was higher than undamaged beam (100 kN).

6 Distributing Sensing

Fiber Bragg grating sensors have been used for the last 20 years, and they have built up a confidence in its performances. FBGs can measure the strain with a similar accuracy to the standard strain gauges and extensometers, and they are also comparable in many aspects from a user's point of view. Indeed, their measurements are local and directional, they require compensation for temperature, they are commonly used by bonding them onto the structure surface and it is also possible to embed the optical fiber in the laminate in the case of composite structures. The main advantages of the FBG over the electrical strain gauges are its reliability for long term measurements; because it is frequency coded, without drifting by aging, and its ability for multiplexing; since several FBGs can be engraved on the same fiber at different positions, resulting in the simultaneous measurement points. The most common procedure for multiplexing is to use a different central frequency for each grating, allowing up to ten FBGs in a single optical fiber, for conventional applications. Another multiplexing

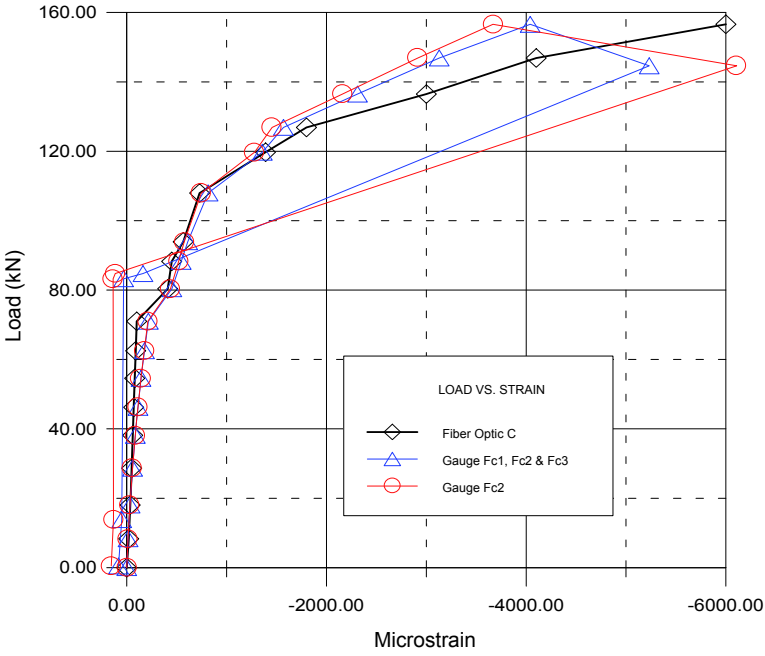

Figure 25. Strain measurements (FOS and strain gauges)

procedure is to have all the gratings with the same central frequency, with a low reflectivity; if gratings are adequately spaced, the return signal will be time-multiplexed, allowing a much larger number of sensors per fiber. The drawback of this procedure is that its response time is smaller, restricting the system to quasi-static applications.

Getting the strains all along the optical fiber, with adequate spatial resolution and strain accuracy, opens new possibilities for structural tests and for structural health monitoring. This is what is understood as 'distributed sensing', with the main difference that the fiber does not need to have local engraved sensors.

The starting point of fiber optic distributed sensing may be identified at the beginning of the 1980s, with the Optical Time-Domain Reflectometer (OTDR) technology, a technique widely used for testing optical cables in the telecommunications industry. The concept is to send a narrow pulse of light through the optical fiber and keep listening for the 'echo' of the backscattered radiation. The detected signal provides a detailed picture of

the local loss distribution or reflections along the fiber caused by any of the attenuation mechanisms or some other non-homogeneities on the fiber. The location of the defect may be calculated by the time of flight. The resolution is in the range of meters, but the operating range was several kilometers, so the technique has been found to be very useful for locating fiber breaks. Figure 26 illustrates the typical graph obtained with conventional equipment. Note the X scale is distance, in km.

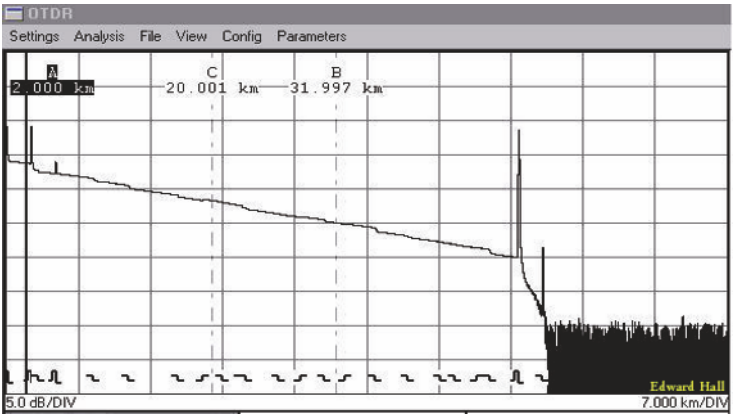

Figure 26. Typical graph obtained with an OTDR, distance vs. Optical losses.

The backscattered radiation. The backscattered light consists of different spectral components due to different interaction mechanisms between the propagating light pulse and the optical fiber. These backscattered spectral components include Rayleigh, Brillouin, and Raman peaks or bands. The Rayleigh backscattering component is the strongest one; it is due to density and composition fluctuations and has the same wavelength as the primary laser pulse. The Rayleigh component controls the main slope of the decaying intensity curve and may be used to identify the breaks and heterogeneities along the fiber.

A small percentage of photons inter-exchange energy with the atoms and new photons with lower (Stokes components) or higher energy are produced. This is known as Raman scattering, the spectral shift is related to the quantum energy absorption/desorption by the atomic bonds of the silica. The intensity of the anti-Stokes component of the Raman radiation increases with temperature, whilst the Stokes component remains stable; the power

ratio between these two peaks, together with the time of the arrival provides information about the local temperature and position respectively. Many commercial systems are currently available to obtain temperature maps over long distances, with important hydrological and environmental applications, including the detection of leakages in buried pipes. These systems basically use a pulsed laser for sending a high power short pulse along the fiber (spatial resolution is related to the width of the pulse, and can hardly be better than 1 meter); at the returning path there is a wavelength separation module, filtering every radiation distinct from the two Raman peaks, and fast photodetectors for each peak. Computing the time for the distance to the light source, and the relative height, resolution in temperature in the range of 0.1 °C, for distances up to 50 km can be achieved.

Raman peaks height was insensitive to strain; in the case of the Brillouin scatter, the wavelength drifting is related to the local temperature and the strain in the fiber. Brillouin-based sensing techniques rely on the measurement of a frequency as opposed to Raman-based techniques which are intensity based. Brillouin based techniques are consequently inherently more accurate and more stable on the long term, since intensity-based techniques suffer from a higher sensitivity to drifts.

There are two types of Brillouin fiber optic sensors. Brillouin Optical Time Domain Reflectometers (BOTDR) resolves the strain or temperature based on Brillouin scattering of a single pulse. Brillouin Optical Time Domain Analysis (BOTDA) uses a more complicated phenomenon known as Stimulated Brillouin Scatter (SBS).

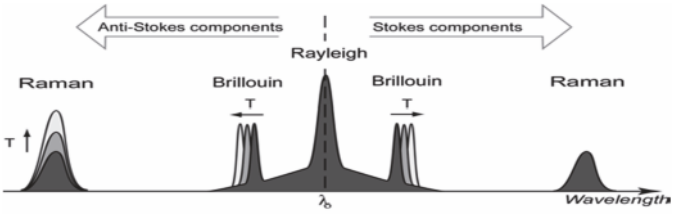

Figure 27. Wavelengths of the backscattered radiation.

Brillouin scattering occurs as a result of an interaction between the propagating optical pulse and the acoustic waves present in the silica fiber, generating frequency shifted components. The diffracted light experiences a Doppler shift since the atoms vibrate at the acoustic velocity in the fiber. The acoustic velocity is directly related to the medium density and depends on both temperature and strain.

The classical BOTDR is essentially an OTDR with a strong filter to avoid the Rayleigh radiation, and with an additional device to discriminate the wavelength of the Brillouin peak. Consequently, it will have the same advantages and limitations of OTDRs: very long interrogation distances, low spatial resolution.

Brillouin Optical Time Domain Analysis (BOTDA) uses a more complicated phenomenon known as Stimulated Brillouin Scatter (SBS). The typical sensor configuration requires two lasers that are directed in opposite directions through the same loop of fiber (one laser operating continuously, the other pulsed). When the frequency difference between the two lasers is equal to the 'Brillouin frequency' of the fiber, there is a strong interaction between the 2 laser beams inside the optical fibers and the enhanced acoustic waves (phonons) generated in the fiber.

This interaction causes a strong amplification of the Brillouin signal which can be easily detected and localized using an OTDR-type sampling apparatus. To make a strain or temperature measurement along the fiber, it is necessary to map out the Brillouin spectrum by scanning the frequency difference (or 'beat' frequency) of the two laser sources and fitting the peak of the Brillouin spectrum to get the temperature and strain information. Current existing BOTDA systems have a spatial resolution in the range of 10 cm, expecting to reach 1 cm in the next equipments generation.

The OBR (Optical Backscatter Reflectometry). The OBR uses swept wavelength interferometry (SWI) to measure the Rayleigh backscatter as a function of length in the optical fiber with high spatial resolution. An external stimulus (like a strain or temperature change) causes temporal and spectral shifts in the local Rayleigh backscatter pattern. These temporal and spectral shifts can be measured and scaled to give a distributed temperature or strain measurement. The SWI approach enables robust and practical distributed temperature and strain measurements in standard fiber with millimeter-scale spatial resolution over tens to hundreds of meters of fiber with strain and temperature resolution as fine as 1 $\mu\varepsilon$ and 0.1 °C.

Figure 28 shows the high spatial resolution achieved. Imagine we have a fiber under test, with four partial reflectors. Each reflector forms an interferometer with the light that goes directly through the other arm of the first coupler. When the system is interrogated by a continuous tunable laser, the reflected signal from each partial reflector is modulated by a unique frequency, longer distances implies faster beatings. A Bragg grating sensor is a partial reflector, with a spectral width much wider that the beating of interferometry, as depicted. Using the Fourier transform, the position of each grating is obtained. With SWI, hundreds of FBG could be multiplexed

in a single optical fiber.

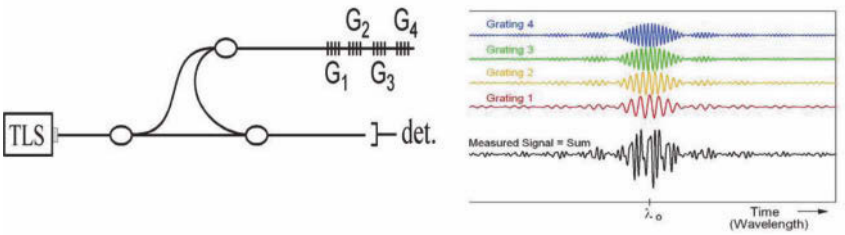

Figure 28. Sketch of the SWI, and the obtained signals.

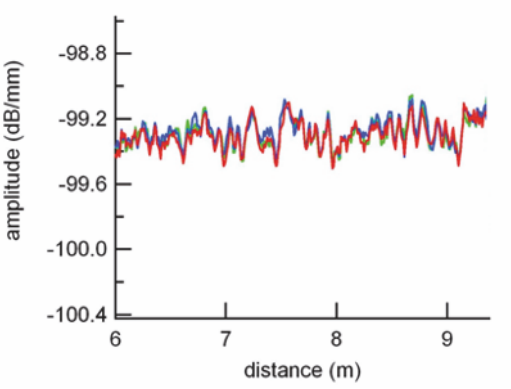

Figure 29. Backscatter Light profile represents a fingerprint that is imprinted in the fiber when it is drawn. Backscatter light presents a high repeatability in absent of external effects.

But there are still more possibilities with this technique. Rayleigh backscatter in optical fiber is caused by random fluctuations in the index profile along the length of the tested fiber. These perturbations will behave as very weak arbitrary FBGs engraved in the fiber all along its length. Shifts in the fiber index of refraction n or in the average perturbation period caused by an external stimulus (like strain or temperature) because shifts in the local spectral frequency of the Rayleigh backscatter. Accumulated changes in the refractive index along the optical path also manifest as a time shift of the Rayleigh backscatter return loss amplitude pattern. Performing a cross correlation on the backscatter amplitude time domain or frequency

domain data accurately measures these spectral and temporal shifts, which are scaled to form distributed temperature or strain measurements.

Consequently, a plain optical fiber behaves as a continuous strain/temperature sensor, with a high spatial accuracy, because it was obtained by interferometric procedures, and with the accuracy in the strain/temperature measurements similar to FBGs. The low power of the reflected signals implies a poor SNR (signal to noise ratio), which can be partially improved by averaging, or repeating the measurements several times, limiting the applications of the technology to almost static tests.

Comparison of technologies. This comparison must be consider very rough, firstly because these technologies are quite new, less than ten years old, and the equipment's performances and prices are evolving very quickly. Secondly, because the definition of performance specifications for distributed sensors is more difficult than for traditional point sensors, since the performance depends on a combination of related measurement parameters. For example, accuracy depends on the spatial resolution, acquisition time, distance range or cumulated loss prior to measurement location.

Two clear conclusions may be drawn from the Table 2:

- Current distributed sensing systems are useful only for static tests. For dynamic tests a multiplexed FBG system is still the only choice.
- The cost of distributed systems is still deterrent if compared to classical extensometry.

7 Applications of Distributed Sensing

Structural tests. The distributed sensing technique may significantly improve the instrumentation of structural tests; instead of bonding a large number of sensors, it will be substituted by bonding one (or several) plain optical fibers in the regions of interest. The main advantage of this technology is that it provides a full coverage of the instrumented area. This issue is of special interest in composite structures, commonly designed with changes of thickness and different stacking sequences. As a consequence, the strain field is not uniform and it is cumbersome to monitor all the critical areas with point strain gauges, since this information is directly obtained with distributed sensing. This technology is also very suitable for detecting local buckling, a problem which presents a great level of difficulty when predicting its character.

In comparison with traditional extensometer sensors, as strain gauges, distributed optical sensors provide a lower price/performance ratio, as it

Table 2. Comparison of technologies.

	FBG	BOTDR	BOTDA	OBR
Strain accuracy	± 1 $\mu\varepsilon$	± 30 $\mu\varepsilon$	± 2 $\mu\varepsilon$	± 1 $\mu\varepsilon$
Spatial resolution	Related to Grating length	0.1 m	0.1 m	0.001 m
Length range	Point sensor	100 km	100 km	100 m
Acquisition time	3 kHz typical sampling rate	0-20 minutes	As low as 1 second	Related to accuracy and length. 30 sec typical
Temperature accuracy	± 0.1 °C	N.A.	± 0.1 °C	± 0.1 °C
Sellers	MicronOptics, Fibersensing, Insensys	Yokogawa, Sensornet, NTT	OZ Optics, Omnisens, Neubrex	LUNA
System cost	3000-6000 Euro	Over 100.000 Euro	Over 200.000 Euro	150.000 Euro

is easy to install, either bonded or embedded, with significant savings in time and money. As no sensor needs to be engraved, standard optical fiber can be used, and it can be obtained with a very competitive price in the market. In spite of these enormous advantages, this technology has not replaced traditional extensometry, mainly due to two reasons; in first place, the purely static acquisition rate, which limits the technique to static tests. It is possible to increase the acquisition rate by using a special optical fiber much more expensive, but it is still unable to be used for aeronautical testing. The second reason is the directional nature of the optical fiber, which makes it extremely difficult to measure the strain field in more than one direction, whilst it is easy to make a rosette with strain gauges. Currently, the state of art of this technology allows it to be used in structural tests, but always as a support for traditional extensometry.

This technique is already used for structural tests of wind turbine blades. Wind turbine blades are the perfect candidates due to their enormous size, because a high number of sensors are required to cover the full structure and the material, with continuous changes of thickness and non-uniform properties.

The results of the structural test of a 43 meters long wind turbine blade

are presented. Up to six standard optical fibers where bonded at the external surface of a wind turbine blade at the following locations: one in the leading edge, two in the pressure side, one in the suction side, and two each side of the trailing edge (see Figure 31). Only one interrogation system was used, the signal was shifted from one fiber to the next one by and optical switch. All these fibers were oriented in the direction of the spar, and run from the root to the edge. Temperature corrections were not needed because the temperature was kept uniform over the structure and constant since the start of load application. In case the temperature would have changed during the tests, a compensation procedure should be done on the data, as with any other strain gauges.

Figure 30. Structural test of a full wind turbine blade.

The concordance amongst the point data obtained with strain gauges and the continuous line obtained with the OBR is excellent; the crooked line is not due to noise, but to the abrupt changes due to ply drops and changes in thickness in the skin of the blade. OBR measurements help the designers detect all the stress concentration areas, even if they were not initially considered of interest. Also, the initiation of the elastic buckling can be clearly detected and located.

Another interesting application under study for wind turbine blades,

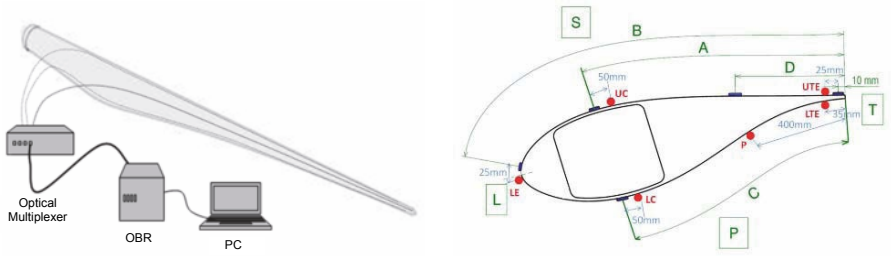

Figure 31. Scheme of fibers mounted in the full blade (left) and in one transversal section (right).

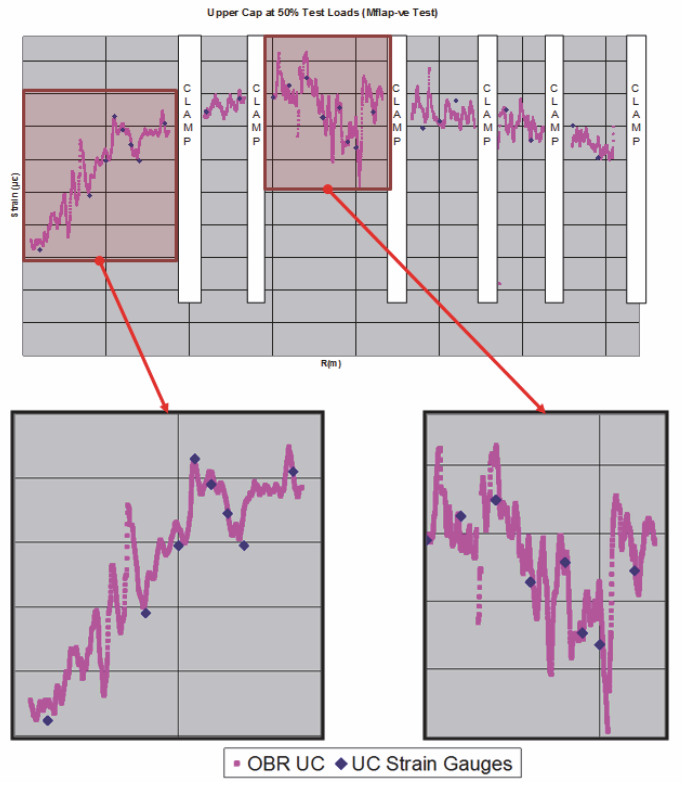

Figure 32. Strain measurements along the length of the blade (above) Details of some areas (below).

not related with structural test, is to monitor temperature during the curing along the full structure. One optical fiber can substitute several thermocouples with a better integration. The first results obtained in the laboratory are very promising.

Damage detection in civil structures. Another field in which distributed sensing can deliver important benefits is civil engineering, since it can be used for monitoring civil structures, such as big buildings, bridges or pipelines. These structures need to be monitored in order to prove their structural safety, and to prevent them from deterioration or damage. One of the key points when monitoring this kind of structures is their large size, bigger than the usual instrumented structures. Unless damages produce a significant change in the stresses path, local sensors, as strain gauges, can only detect damages in their nearest area, and a large amount of sensors is required to cover the full structure.

Distributed optical sensors provide a high density sensor network to cover the full structure at a low price, as standard single-mode fiber is used as sensor. However, the capability to easily manage a huge number of sensors using distributed sensing is not new. Up to now distributed sensing techniques have not found a widespread usage in civil structural applications due to their insufficient resolution and their limitation to be used in static examples to measure average strain, due to the poor resolution of previous distributed techniques. One of the applications that have attracted most interest is pipeline crack monitoring. Small cracks can be detected due to the large increase of the average strain at the region of the fiber where the crack was produced. Several papers have used this approach; the OBR improves the spatial resolution of the mentioned technologies.

A similar experimental test was carried out on a reinforced concrete slab in the Structural Technology Laboratory of UPC (Polytechnic University of Catalunya, Spain) . One fiber was bonded on the surface of a reinforced concrete slab of 5.60 x 1.60 m. The fiber was bonded along the longitudinal direction, with two lines in the upper side and another two lines bonded on the lower side.

Strain sensors are not commonly used in the surface of concrete slabs since material heterogeneity due to the presence of aggregates of several sizes promotes a non uniform strain field in the surface. In Figure 34 the strain field in the upper side at different load levels can be observed. Strain grows uniformly, with irregularities near the load application region.

At the bottom side, tensile stresses promote crack appearance, and the strain chart is quite different. Data measured with optical fibers detects strain concentration due to cracks, even at low load levels. It is possible to

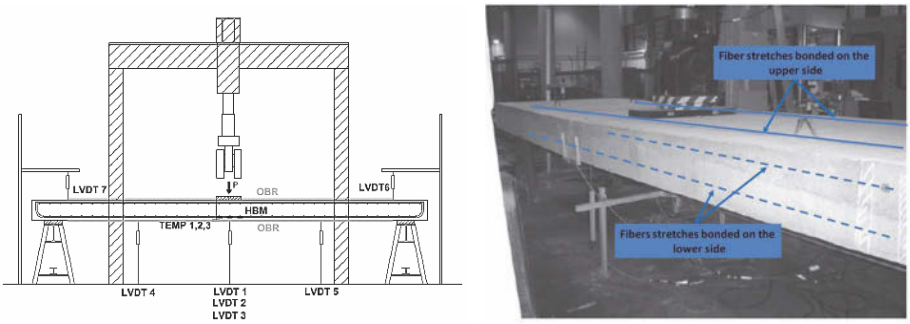

Figure 33. Test scheme (left). Location of optical fiber on concrete slab right).

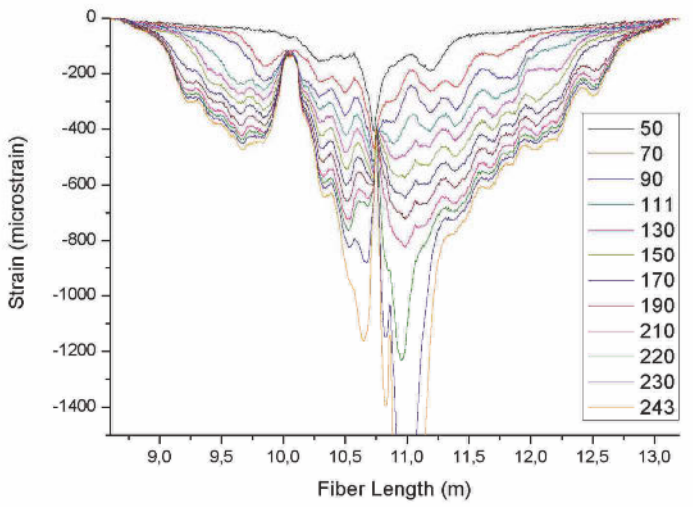

Figure 34. Strain field in the upper side of the slab at different load levels.

track crack appearance with increasing load levels, and detect crack location even in severe cracking conditions (Figure 35 and Figure 36).

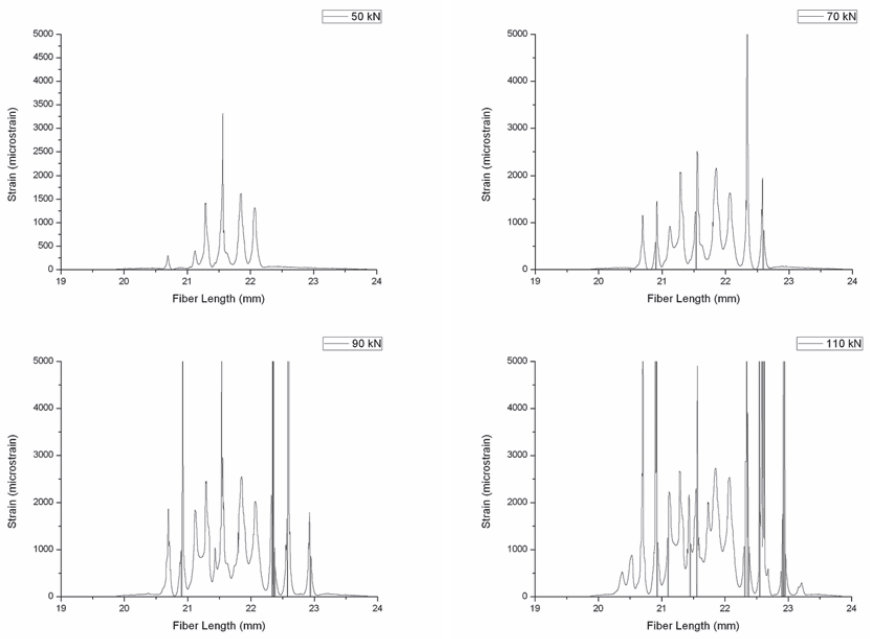

Figure 35. Strain measured with OBR along the lower side for different load levels: 50 kN (up, left), 70 kN (up, right), 90 kN (down, left) and 110 kN (down, right).

Damage detection in composites laminates. High accuracy in strain resolution and a spatial resolution better than 1 mm allows an ultra-high density sensor network with a single optical fiber, with such good performances that it may even detect the strain changes induced by a delamination.

Strain changes induced by a delamination are related to the residual strains built in the laminate during the curing and have only a local influence, limited to the delamination area. For these reasons a high-density strain sensor network is required, and formerly SHM techniques for delamination detection were not based on strain measurements.

To study the changes in the strain field promoted by impact damages, plates 150 mm long and 100 mm wide were manufactured with embedded

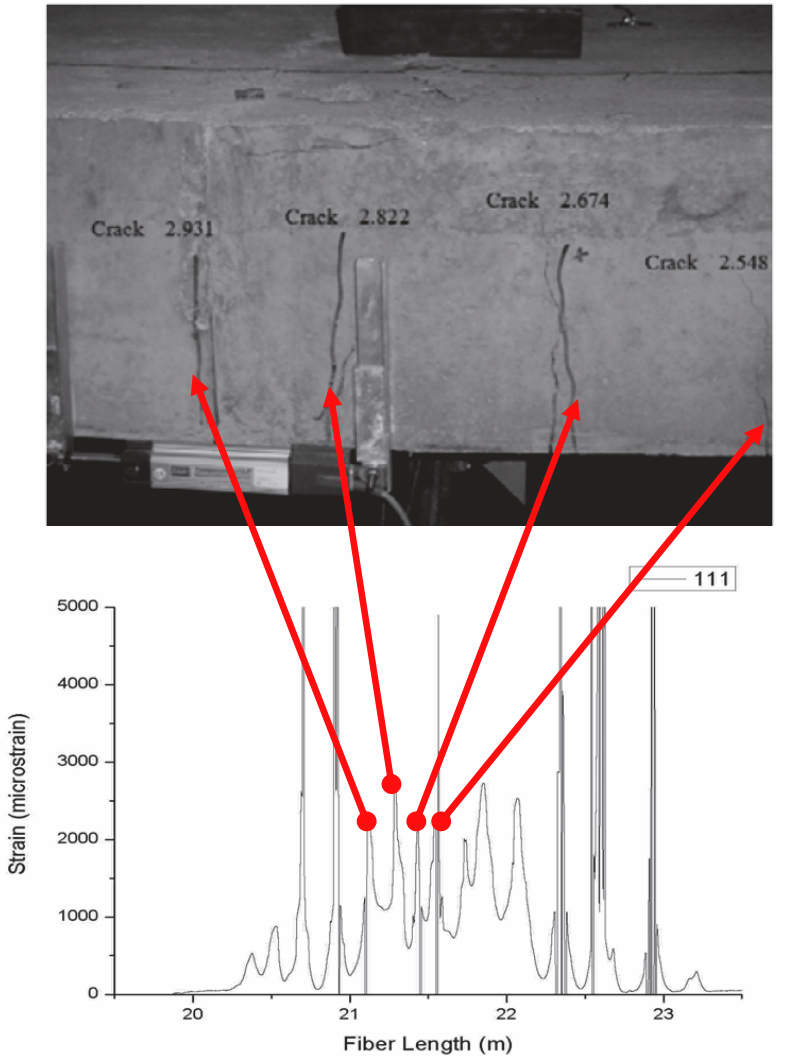

Figure 36. Correspondence between strain concentration peaks (down) and cracks in the concrete slab (up).

optical fiber. Plates were built with carbon/epoxy tape AS4/8552 with $[0_2,90_2,0_2]$ cross ply lay-up. Optical fibers were embedded along the longitudinal central line between plies with the same orientation. The embedded optical fiber has polyimide coating with a final diameter of 140 ± 2 $\mu\varepsilon$. This type of coating is recommended for measuring the strain gradients due to their small thickness.

The first plate was subject to a 2.4 J impact at the middle of the plate. With this energy level, fiber C-1 (embedded in the opposite side to the impact) was broken. The strain readings at the other two fibers show a peak in damage location with similar strain level. In Figure 37 the C-Scan inspection after the damage can be observed. The strain field is mainly affected in the delamination area, with a maximum of nearly 500 $\mu\varepsilon$. One of the fibers, the one embedded in the middle of the plate, between the 90° plies, presents a strain field variation limited to the delamination area. The other fiber, embedded between two 0° plies, is mainly affected in the delamination area, but strain field changes affect also the close delamination region. With an impact of 4.4 J, all the fibers were broken. Test performed with fibers with acrylate coating of 250 $\mu\varepsilon$ did not show an improvement of resistance to impacts.

To avoid fiber breakage, impacts were performed 10 mm away from the fiber line (see Figure 38 Left). In this case, a growing delamination was monitored. In spite of the delamination size growing, the fiber length inside the delamination remained nearly constant. Figure 39 shows the strain along the different fibers: strain fields are similar in all of them, and present a maximum strain level in the delamination area. In these tests, all of the fibers show also an influence in the close strain field. Additionally, impact energy has no effect in the strain field level. Impacts were done for increasing energy levels (2.4, 4.4, 6.3 and 12 J).

Strain results can be explained by the influence of the cracks induced in the 90° plies, as the residual strain of these plies in the direction of the fiber is mainly compression. After the cracks appear, residual stresses are relaxed and affect the 0° plies too.

Strain measurements obtained from the full surface can be used to create a strain map of the structure. In case that damage promotes a change in the strain field, it is possible to obtain an image that represents the state of the structure. Figure 41 shows the effect of a delamination in a cross ply laminate of 200 x 200 mm. Strain data was obtained from a fiber in a zig-zag configuration that covered one of the sides.

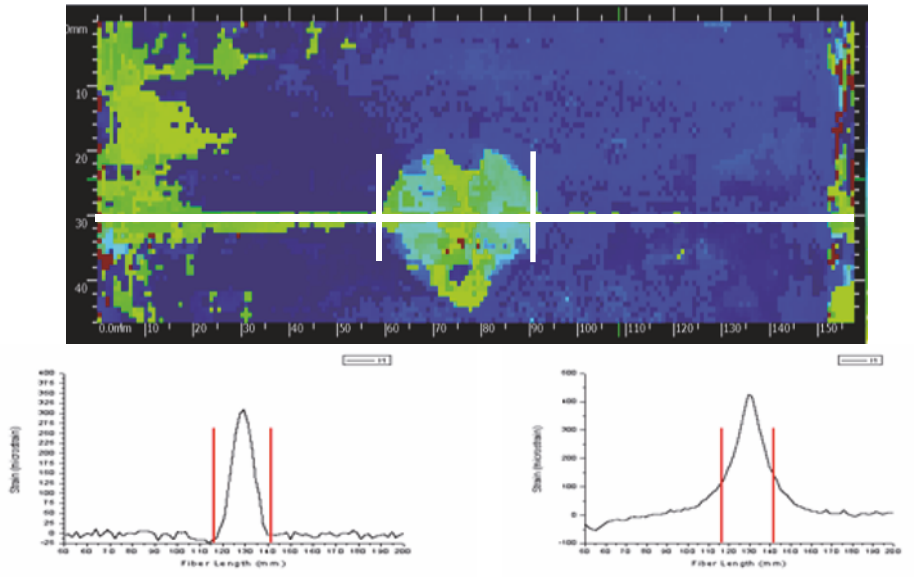

Figure 37. Ultrasonic inspection C-Scan after 2.4 J impact (Up). Strain measures of fibers C-2 (down, left) and C-3 (down, right).

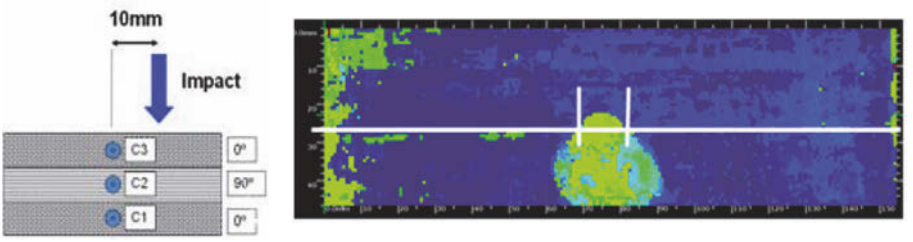

Figure 38. Scheme of test (left). Ultrasonic inspection C-Scan after 4.4 J impact (Right).

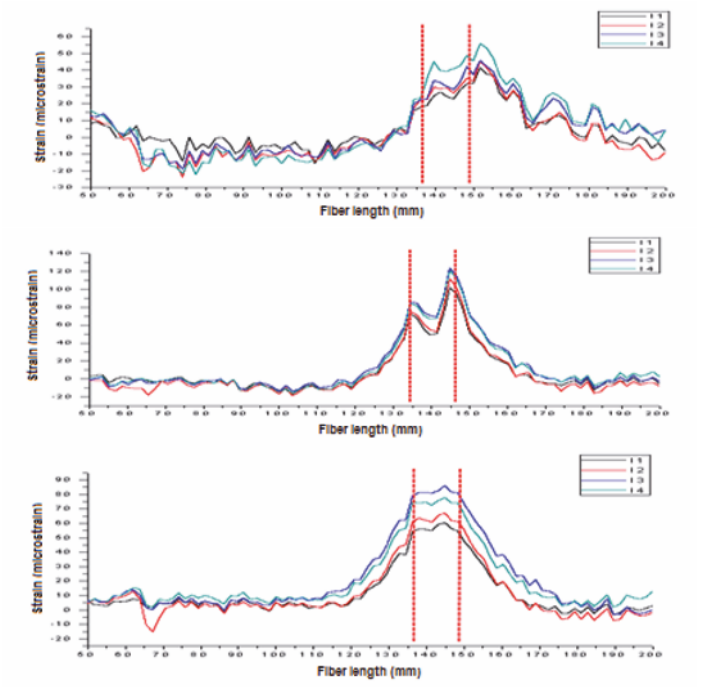

Figure 39. Strain distribution along the fiber after different impact levels for fiber C-1 (Up), C-2 (Middle) and C-3 (down).

8 Final Comments

The technology of fiber optic sensors, and particularly of the fiber Bragg gratings, is well matured for strain monitoring at a few points, and can be used for load monitoring in conventional and advanced structures. It offers several important advantages over conventional strain sensing, namely:

- Low size and weight, embeddable capability, single ended cabling.
- Long term stability, it can be used for load monitoring during the whole structural life.
- Inherent multiplexability, typical 10 sensors/fiber without decreasing reading speed.
- Immune to electromagnetic noise, able to work in harsh or explosive environment

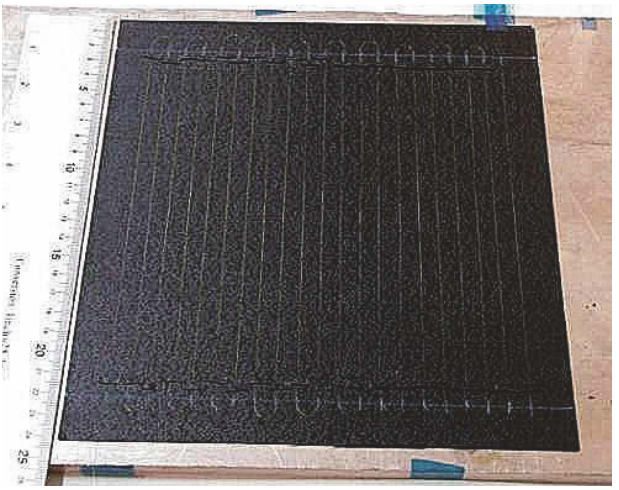

Figure 40. Fiber in a uniform zig-zag distribution in a composite laminate.

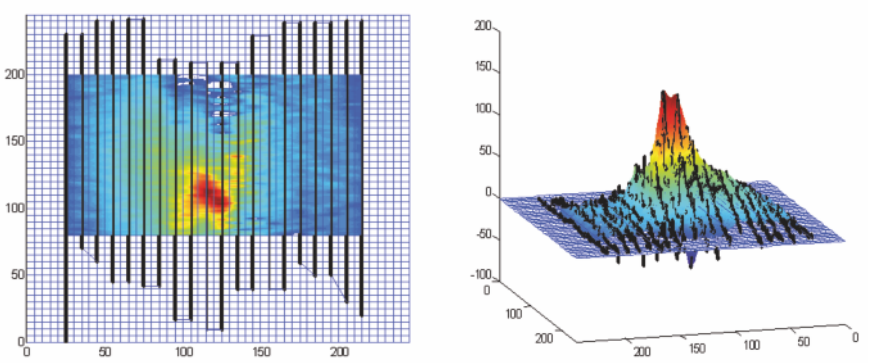

Figure 41. Strain map due to a delamination in 2D (left). And 3D (right).

Current efforts address to development and demonstration of large sensor arrays, affording a detailed map of the strain field. in a complex structure, such as a ship, an aircraft or a bridge. This would require new optoelectronics and signal processing systems, able to handling at high speed the information coming from several hundreds of sensing points, compressing this information to the significant events. This is needed if damage detection is intended, because in continuous structures a local damage will produce a very small change in the global strain field. Only considering the dynamic response or the transients strains, some information can be derived about damage occurrence.

While FBG does local strain measurements, similarly to strain gauges, new possibilities are opened by the distributed sensing, giving the information all along the optical fiber. Structural tests may be instrumented with greater details, and crack occurrence will be easily detected, as long as the crack crosses the optical fiber path.

Only the strain and temperature response of FBG was discussed in this chapter. Additionally, fiber optic sensors may afford very valuable information on chemical processes, such as corrosion in metals, degradation phenomena in concrete structures, or for the resin curing in composite materials. This is a very active research area, and combined to process modeling is paving the way to the intelligent materials processing.

Bibliography

M. Amano, Y. Okabe, N. Takeda, and T. Ozaki. Structural health monitoring of an advanced grid structure with embedded fiber bragg grating sensors. *Struct. Health Monit*, 6:309–316, 2007.

D.C. Betz, G. Thursby, B. Culshaw, and W.J. Staszewski. Acousto-ultrasonics sensing using fiberbragg grating. *Smart Mater. Struct*, pages 122–128, 2003.

D.D. Betz, W.J. Staszewski, G. Thursby, and B. Culshaw. Multi-functional fibre bragg grating sensors for fatigue crack detection in metallic structures. *J. Aerospace Eng*, 12:453–461, 2006.

K. Chandler, S. Ferguson, T. Graver, A. Csipkes, and A. Mendez. On-line structural health and fire monitoring of a composite personal aircraft using an fbg sensing system. In *Proc. SPIE*, 2008.

B.A. Childers, M.E. Froggatt, S.G. Allison, T.C. Moore, D.A. Hare, C.F. Batten, and D.C. Jegley. Use of 3000 bragg grating strain sensors distributed on four eight-meter optical fibers during static load testing of a composite structure. 2001.

C. Connolly. Fibre-optic-based sensors bring new capabilities to structural monitoring. *Sensors Rev*, 26:236–243, 2006.

G. Coppola. Analysis of feasibility on the use of fiber bragg grating sensors as ultrasound detectors. In *Proc. SPIE*, pages 224–232, 2001.

B. Culshaw and A. Kersey. Fiber-optic sensing: A historical perspective. *IEEE/OSA J. Lightwave Tech*, 26:1064–1078, 2008.

M. Frövel, I. Fernandez, J. M. Pintado, J. A. Güemes, and J. M. Menéndez. Monitoring the buckling and postbuckling behaviour of stiffened cfrp panels with fibre optic sensors. In *European COST F3 Conference on System Identification and Structural Health Monitoring, Proceedings of the Conference*, pages 539–548, 2000.

N. Fuerstenau, D. D. Janzen, and W. Schmidt. Flight tests of a fiber-optic interferometric strain gauge. In *Fiber optic smart structures and skins V; Proceedings of the Meeting, SPIE-1798*, pages 295–301, 1992.

B. Glisic and D. Inaudi. *Fibre Optic Methods for Structural Health Monitoring*. John Wiley and Sons, Ltd, 2007.

J.A. Güemes and J. M. Menéndez. Fiber-optics sensors. In D. Balageas, C.P. Fritzen, and J.A. Güemes, editors, *Structural Health Monitoring*. Wiley, 2006.

J.A. Güemes, S. Díaz-Carrillo, and J. M. Menéndez. Measurement of strain distribution in bonded joints by fiber bragg gratings. In *Smart Structures and Materials; Proceedings of the Meeting, SPIE-3330*, pages 264–271, 1998a.

J.A. Güemes, S. Díaz-Carrillo, J. M. Menéndez, C. Pardo de Vera, P. Vionis, R. Scherer, D. Bercebal, and A. Cuerva. Strain and damage monitoring of wind turbine blades by piezoelectrics and fiber optic sensors. In *Proceedings of the ECCM-8 European Conference on Composite Materials*, pages 357–364, 1998b.

J.A. Güemes, J. M. Menéndez, M. Frovel, I.Fernandez, and J.M Pintado. Experimental analysis of buckling in aircraft skin panels by fibre optic sensors. *Smart Materials and Structures.*, 10:490–496, 2001.

J.A. Güemes, A. Fernandez, and B. Soller. Optical fiber distributed sensing. physical principles and applications. *J. Structural Health Monitoring*, 9: 233–245, 2010.

H. Guo, Y. DaiÂ¡, G. Xiao, N. Mrad, and J. Yao. Interrogation of a long-period grating using a mechanically scannable arrayed waveguide grating and a sampled chirped fiber bragg grating. *Opt. Lett.*, 33:1635–1637, 2008.

K.O. Hill and G. Meltz. Fiber bragg grating technology fundamentals and overview. *IEEE/OSA J. Lightwave Tech*, 15:1263–1276, 1997.

K.O. Hill, Y. Fujii, D. D. Johnson, and B. S. Kawasaki. Photosensitivity in optical fiber waveguides: application to reflection filter fabrication. *Applied Physics Letters*, 32:647–649, 1978.

A. Hongo, S. Kojima, and S. Komatsuzaki. Applications of fiber bragg grating sensors and high-speed interrogation techniques. *Struct. Control Health Monit.*, 12:269–282, 2005.

R. L. Idriss, M. B. Kodindouma, A. D. Kersey, and M. A. Davis. Multiplexed bragg grating optical fiber sensors for damage evaluation in highway bridges. *Smart Materials and Structures*, 7:209–216, 1998.

R. Isago and K. Nakamura. A high reading rate fiber bragg grating sensor system using a high-speed swept light source based on fiber vibrations. *Meas. Sci. Tech.*, 20:1–5, 2009.

M. Leblanc, S. Y. Huang, M. M. Ohn, A. Güemes, and A. Othonos. Distributed strain measurement based on a fiber bragg grating and its reflection spectrum analysis. *Optical Letters*, 21:1405–1407, 1996.

B. Lee. Review of the present status of optical fibre sensor. *Opt. F iber Tech*, 9:57–79, 2003.

Z.Q. Luo, C.C. Ye, Z.P. Cai, X.Z. Dai, Y. Kang, and H.Y. Xu. Numerical analysis and optimization of optical spectral characteriscs of fiber bragg gratings modulated by a transverse acoustic wave. *Appl. Opt*, 46:6959–6965, 2007.

M. Majumder, T.K. Gangopadhyay, A.K. Chakraborty, K. Dasgupta, and D.K. Bhattacharya. Fibre bragg gratings in structural health monitoring: Present status and applications. *Sens. Actuat. A*, 147:150–164, 2008.

R. M. Measures. Smart structures with nerves of glass. *Progress on Aerospace Science*, 26:289–351, 1989.

R.M. Measures. *Structural Monitoring with Fiber Optic Technology.* Academic Press, 2004.

G. Meltz, W. Morey, and W. H. Glenn. Formation of bragg gratings in optical fibers by a transverse holographic method. *Optics Letters*, 14: 823–825, 1989.

J. M. Menéndez and J. A. Güemes. Bragg-grating-based multiaxial strain sensing: its application to residual strain measurement in composite laminates. In *Smart Structures and Materials 2000; Proceedings of the Meeting, SPIE-3986*, pages 271–281, 2000.

J. M. Menéndez and J.A. Güemes. Strain measurements inside thick cfrp laminates at the vicinity of bolted joints. In *Smart Structures and Materials; Proceedings of the Meeting, SPIE-3670*, pages 184–194, 1999.

J. M. Menéndez and J.A. Güemes. Bragg grating-based multiaxial strain sensing: its application to residual strain measurement in composite laminates. 2008.

A. Minardo, A. Cusano, R. Bernini, L.G. Zeni, and M. Giordano. Response of fiber bragg gratings to longitudinal ultrasonic waves. *IEEE Trans. Ultrason. Ferroelect. F req. Control*, 52:304–312, 2011.

W.W. Moorey, G.A. Ball, and H. Singh. Applications of fibre grating sensors. *Proc. SPIE*, pages 2–7, 1996.

N. Mrad. Potential of bragg grating sensors for aircraft health monitoring. *Trans. CSME*, 31:1–17, 2007.

N. Nakamura, T. Ogisu, H. Yoneda, Y. Okabe, N. Takeda, and Sakurai. Impact monitoring of the aircraft composite structure using fbg sensor/pzt actuator hybrid sensor system. In *Proc. SPIE*, 2007.

I. Perez, H.L. Cui, and E. Udd. Acoustic emission detection using fiber bragg gratings. pages 209–215, 2001.

D. Philen, I. White, J. Kuhl, and S. Mettler. Single-mode fiber otdr: Experiment and theory. *IEEE J. Quant. Elect*, 18:1499–1508, 2003.

X.L. Qing, A. Kumar, C. Zhang, I.F. Gonzalez, G.P. Guo, and F.K. Chang. A hybrid piezoelectric/fiber optic diagnostic system for structural health monitoring. *Smart Mater. Struct.*, 14:98–103, 2005.

F. Rodríguez-Lence, P. Muñoz-Esquer, J. M. Menéndez, C. Pardo de Vera, S. Díaz, and J. A. Güemes. Smart sensors for resin flow and composite cure monitoring. In *Proceedings of the Ninth Conference on Artificial Intelligence, ICCM-12*, 1999.

B. E. A. Saleh and M. C. Teich. *Fundamental of Photonics.* Wiley Interscience, 1991.

P. Schindler, R. May, and R. O. Claus. Optical fiber sensors for damage analysis in aerospace materials. *NASA Technical Report NASA-CR-199981*, pages 1–64, 1995.

L.Y. Shao, X.Y. Dongand A.P. Zhang, H.Y Tam, and S.L. He. High resolution strain and temperature sensor based on distributed bragg reflector fiber laser. *IEEE Photon. Tech. Lett.*, 19:1598–1600, 2007.

H. Soejima, T. Ogisu, H. Yoneda, Y. Okabe, N. Takeda, and Y. Koshioka. Demonstration of detectability of shm system with fbg/pzt hybrid system in composite wing box structure. 2008.

D.M. Spirit and L.C. Blank. Raman-assisted long-distance optical time domain reflectometry. *Elect. Lett*, 25:1687–1689, 2002.

M.D. Todd, J.M. Nichols, S.T. Trickey, M. Seaver, C.J. Nichols, and L.N. Virgin. *Bragg grating-based fibre optic sensors in structural health monitoring.* Phil. Trans. Roy. Soc. A, 2007.

E. Udd. Embedded sensors make structures 'smart'. *Laser Focus*, pages 135–, 1988.

G. Wild and S. Hinckley. Acousto-ultrasonic optical fiber sensors: Overview and state-of-the-art. *IEEE Sens. J*, 8:1184–1193, 2008.

G. Xiao, P. Zhao, F. Sun, Z. Lu, Z. Zhang, and C. Grover. Interrogating fiber bragg grating sensors by thermally scanning an arrayed waveguide grating based demultiplexer. *Opt. Lett.*, 29:2222–2224, 2004.

G. Zhou and L.M. Sim. Damage detection and assessment in fibre-reinforced composite structures with embedded fibre optic sensors review. *Smart Materials and Structures.*, 11:925–939, 2002.